Ribbon turbulence

Antoine Venaille, Louis-Philippe Nadeau, and Geoffrey Vallis

Citation: Physics of Fluids (1994-present) **26**, 126605 (2014); doi: 10.1063/1.4904878
View online: http://dx.doi.org/10.1063/1.4904878
View Table of Contents: http://scitation.aip.org/content/aip/journal/pof2/26/12?ver=pdfcov
Published by the AIP Publishing

PHYSICS OF FLUIDS **26**, 126605 (2014)

Ribbon turbulence

Antoine Venaille,[1,a)] Louis-Philippe Nadeau,[2] and Geoffrey Vallis[3]
[1]*Laboratoire de Physique de l'École Normale Supérieure de Lyon, CNRS and Université de Lyon, 46 Allée d'Italie, 69007 Lyon, France*
[2]*EAPS, MIT, 77 Massachusetts Avenue, Cambridge, Massachusetts 02139-4307, USA*
[3]*CEMPS, University of Exeter, Exeter EX4 4QF, United Kingdom*

(Received 11 June 2014; accepted 5 December 2014; published online 30 December 2014)

We investigate the non-linear equilibration of a two-layer quasi-geostrophic flow in a channel with an initial eastward baroclinically unstable jet in the upper layer, paying particular attention to the role of bottom friction. In the limit of low bottom friction, classical theory of geostrophic turbulence predicts an inverse cascade of kinetic energy in the horizontal with condensation at the domain scale and barotropization in the vertical. By contrast, in the limit of large bottom friction, the flow is dominated by ribbons of high kinetic energy in the upper layer. These ribbons correspond to meandering jets separating regions of homogenized potential vorticity. We interpret these results by taking advantage of the peculiar conservation laws satisfied by this system: the dynamics can be recast in such a way that the initial eastward jet in the upper layer appears as an initial source of potential vorticity levels in the upper layer. The initial baroclinic instability leads to a turbulent flow that stirs this potential vorticity field while conserving the global distribution of potential vorticity levels. Statistical mechanical theory of the $1^1/_2$ layer quasi-geostrophic model predicts the formation of two regions of homogenized potential vorticity separated by a minimal interface. We explain that cascade phenomenology leads to the same result. We then show that the dynamics of the ribbons results from a competition between a tendency to reach the equilibrium state and baroclinic instability that induces meanders of the interface. These meanders intermittently break and induce potential vorticity mixing, but the interface remains sharp throughout the flow evolution. We show that for some parameter regimes, the ribbons act as a mixing barrier which prevents relaxation toward equilibrium, favouring the emergence of multiple zonal (eastward) jets. [http://dx.doi.org/10.1063/1.4904878]

I. INTRODUCTION

A striking property of observed oceanic mesoscale turbulence (from 10 to 1000 km) is the ubiquity of jets with a typical width of order the internal Rossby radius of deformation, R. In quasi-geostrophic theory $R = NH/f$, where N is the buoyancy frequency, H is a vertical scale, and f is the Coriolis parameter, and in the ocean $R \sim 50$ km. These jets are robust coherent structures but with high variability characterized by strong meanders—as in, for example, the cases of the Gulf-Stream or the Kuroshio. Sometimes these meanders break into an isolated vortex, in which case the jets are curled into rings that literally fill the oceans. What sets the strength, the horizontal size and the vertical structure of mesoscale eddies is a longstanding problem in physical oceanography. Here we address this question in a two-layer quasi-geostrophic model, with a particular focus on the role of bottom friction. We consider the equilibration of an initial perturbation in a channel with an imposed constant vertical shear U in the zonal (eastward) direction. This model might be considered as one of the elementary building blocks of a hierarchy of more complex models that

a)Electronic mail: antoine.venaille@ens-lyon.fr

describe oceanic or atmospheric turbulence.[1,2] One motivation for this model is that the main source of energy for these turbulent flows comes from baroclinic instability that releases part of the huge potential energy reservoir set at large scale by wind forcing at the surface of the oceans or solar heating in the atmosphere.[3]

Bottom friction is the main sink of kinetic energy and without it there will be no nonlinear equilibration, so it is important to fully understand its role. A crude but effective model of that bottom friction, based on Ekman-layer dynamics, is simply linear drag with coefficient r. Given this, the two-layer model has two important nondimensional parameters: the ratio R/L_y, with L_y the width of the channel, and the ratio rR/U which is a measure of the bottom friction time scale to an inertial time scale based on the Rossby radius of deformation. The inertial time scale R/U may alternatively be interpreted as the Eady time scale, namely, the baroclinic instability time scale in the low friction limit. There are other important parameters if the Coriolis parameter is allowed to vary but these are not our particular concern here.

In the low bottom friction limit, classical arguments based on cascade phenomenology predict an inverse cascade of kinetic energy in the horizontal with a concomitant tendency toward barotropization in the vertical, i.e., the emergence of a depth independent flow.[4–6] In a closed finite-sized domain, the inverse energy cascade in the horizontal leads to condensation of the eddies at the domain scale. The intermediate regime ($rR/U \sim 1$) has been studied by Thompson and Young,[7] using vortex gas kinetics since the flow is made in that case of a multitude of isolated vortices or dipoles. The high bottom friction limit has been studied numerically by Arbic and Flierl,[8,9] who also proposed scaling arguments for the vertical structure of the flow. They observed the spontaneous formation of coherent jets in the upper layer. Arbic and Flierl[9] noticed that these coherent jets looked like localized, thin, and elongated ribbons of high kinetic energy. The typical width of these jets was given by the Rossby radius of deformation of the upper layer and was, therefore, much sharper than jets. These ribbons were reported to interact together in a seemingly erratic way through meandering, pinching, coalescence, and splitting of the regions separating them. Accordingly, the high bottom friction regime will be referred to in the following as "ribbon turbulence."

The numerical results of Thompson and Young,[7] Arbic and Flierl[9] were all performed in a doubly periodic domain and one novelty of our work is to consider a channel geometry. A particular advantage of the channel geometry is that, with a proper definition of the potential vorticity, the non-linear dynamics of a perturbation around a prescribed mean-flow is equivalent to a free decay experiment in which the initial condition is given by the prescribed mean flow. In particular, the dynamics in the upper layer can be recast in the form of an advection equation for the potential vorticity field, without sources or sinks, whereas in a doubly periodic geometry the beta term associated with the prescribed eastward jet must be subtracted off in order to avoid a potential vorticity discontinuity at the boundary. We will discuss the physical consequences of these conservation laws in the low bottom friction limit and in the high bottom friction limit. This will allow us to revisit the barotropization process in the weak bottom friction limit and the emergence of ribbons in the high bottom friction limit. In particular, we will interpret the emergence of ribbons as a tendency to reach a statistical equilibrium state. Statistical mechanical theory provides predictions for the self-organization properties of two-dimensional and quasi-geostrophic flows and was initially proposed by Miller[10] and Robert and Sommeria.[11] The theory applies to freely evolving flow (without forcing and dissipation), explains self-organization of the flow into the most probable state as the outcome of turbulent stirring, and allows the computation of this most probable state. In practice, the computation of the statistical equilibria requires the knowledge of a few key parameters such as the energy and the global potential vorticity distribution as an input.

When bottom friction is large, the two-layer quasi-geostrophic dynamics is strongly dissipated, and one might expect that any prediction of the equilibrium theory applied to this two-layer flow would fail. However, we will argue that key features of the equilibrated states, including the emergence of ribbons, can be accounted for by considering equilibrium states of $1\frac{1}{2}$ layer quasi-geostrophic turbulence, which amounts to assuming that only the upper layer is "active." It has been shown previously that when the Rossby radius is small, equilibrium states of a $1\frac{1}{2}$ layer quasi-geostrophic model contain two regions of homogenized potential vorticity, with a thin

interface between these regions.[12] We will explain why this is relevant to describe the emergence of ribbons and provide a complementary point of view based on cascade arguments. We will go further than the application of equilibrium statistical mechanics in order to account for some of the dynamical aspects of the ribbons. In particular, we will show that the observed meanders of the ribbons cannot be explained in the framework of $1^1/_2$ layer quasi-geostrophic model, but must be accounted for by the baroclinic instability of the ribbons in the framework of a two-layer quasi-geostrophic model. We will also see that once a ribbon is formed, it may act as a mixing barrier and prevent relaxation towards the equilibrium state. For this reason, more than two regions of homogenized potential vorticity can coexist for some range of parameters. We will relate this observation to the emergence of multiple zonal jets in this flow model.

The paper is organized as follows. The basic model is presented in Sec. II along with a discussion of the physical consequences of existing conservation laws for the dynamics. In Sec. III, we review existing results based on cascade arguments and statistical mechanics approaches and give predictions for the flow structure at large times. These predictions are tested against numerical simulations in Sec. IV, and we conclude in Sec. V.

II. BAROCLINIC TURBULENCE IN A TWO-LAYER QUASI-GEOSTROPHIC FLOW

A. Two layer quasi-geostrophic flows in a channel

We consider a two-layer quasi-geostrophic model on an f-plane in a channel periodic in the x direction and of size $(L_x \times L_y)$ (Fig. 1(a)). The relative depths of the upper and lower layers are $\delta = H_1/H$ and $1-\delta = H_2/H$, respectively, with H the total depth. Consequently, the internal Rossby radius of deformation of the upper and the lower layers are $R_1 = \delta^{1/2}R$ and $R_2 = (1-\delta)^{1/2}R$, respectively, with $R = (Hg')^{1/2}/f_0$, where g' is the reduced gravity between the two layers and f_0 is the Coriolis parameter. The dynamics is given by the advection in each layer of the potential vorticity fields q_1, q_2 by a non-divergent velocity field which can be expressed in terms of a streamfunction Ψ_1, Ψ_2,

$$\partial_t q_1 + J(\Psi_1, q_1) = -A_h \nabla^6 \Psi_1, \tag{1}$$

$$\partial_t q_2 + J(\Psi_2, q_2) = -A_h \nabla^6 \Psi_2 - r\nabla^2 \Psi_2, \tag{2}$$

where A_h is a lateral bi-harmonic viscosity coefficient, r is a bottom drag coefficient, and $J(a,b) = \partial_x a \partial_y b - \partial_y a \partial_x b$ is the Jacobian operator. The velocity field in each layer is given by $U_i = -\partial_y \Psi_i$, $V_i = \partial_x \Psi_i$, for $i = 1, 2$. The potential vorticity fields are expressed as the sum of a relative

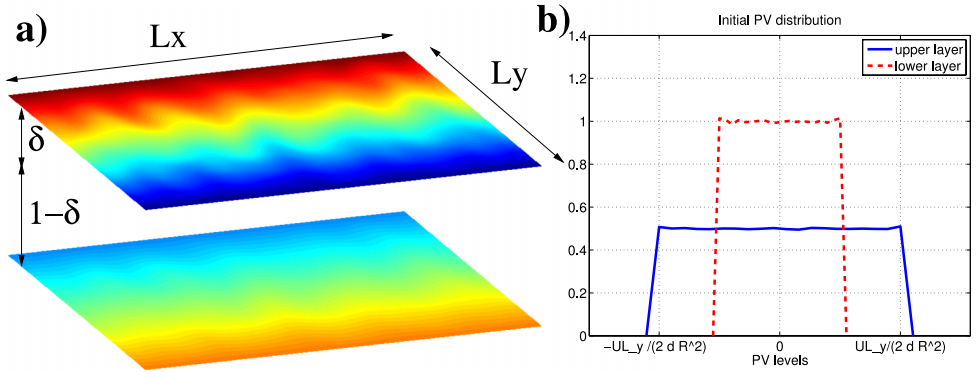

FIG. 1. Sketch of the numerical experiment. Left panel: potential vorticity field at the beginning of the simulation, when the most unstable mode starts to grow, in the case without bottom friction. Right panel: global distribution of potential vorticity levels at t=0, which is the same whatever the bottom friction value.

vorticity term $\zeta_i = \nabla^2\Psi_i$ and a stretching term involving the Rossby radius of deformation R

$$q_1 = \nabla^2\Psi_1 + \frac{\Psi_2 - \Psi_1}{\delta R^2}, \tag{3}$$

$$q_2 = \nabla^2\Psi_2 + \frac{\Psi_1 - \Psi_2}{(1-\delta)\,R^2}. \tag{4}$$

These equations must be supplemented with boundary conditions. The flow is periodic in the x direction, and there is no flow across the wall at the northern and the southern boundaries. This impermeability constraint amounts to assuming that $\Psi_{1,2}$ is a constant at the northern and the southern boundaries. Four equations are then needed to determine these constants. Two equations are given by mass conservation, which imposes the constraints

$$\int_{\mathcal{D}} \mathrm{d}x\mathrm{d}y\Psi_1 = \int \mathrm{d}x\mathrm{d}y\Psi_2 = 0. \tag{5}$$

Two additional equations are obtained by integrating over one line of constant latitude (constant y) the zonal projection (along $\mathbf{e}_x$) of the momentum equations in each layers. Let us consider the particular case where the line of constant latitude is the southern boundary, and let us call $\Gamma_i = \int_0^{L_x} \mathrm{d}x U_i(x,0)$ the circulation along this boundary. Then the two additional equations are

$$\frac{d\Gamma_1}{dt} = -A_h\left(\int_0^{L_x} \mathrm{d}x\nabla^4 U_1\Big|_{y=0}\right), \quad \frac{d\Gamma_2}{dt} = -A_h\left(\int_0^{L_x} \mathrm{d}x\nabla^4 U_2\Big|_{y=0}\right) - r\Gamma_2, \tag{6}$$

see Pedlosky[13] for further details on the quasi-geostrophic dynamics in an open channel.

In the absence of small scale dissipation (i.e., when $A_h = 0$), the dynamics is fully determined by Eqs. (1), (2), (6), and (5). When small scale dissipation is taken into account (i.e., when $A_h \neq 0$), additional boundary conditions are required due to the higher order hyperviscous term appearing in Eqs. (1), (2), and (6). We will consider a free slip condition $\nabla^2\psi_i = 0$ along each solid wall, which ensures no flux of tangential momentum through the walls, supplemented with the condition $\nabla^4\psi_i = 0$, which ensures that the presence of hyperviscosity does not induce energy production at the solid walls. These boundary conditions are sufficient to fully determine the dynamics, see, e.g., McWilliams, Holland, and Chow[14] and Holland,[15] for more details.

B. Evolution of a perturbation around a prescribed eastward jet

We impose the existence of a constant eastward flow in the upper layer with a lower layer at rest ($\overline{\Psi}_1 = -U\,y$, $\overline{\Psi}_2 = 0$). We denote ψ_1 and ψ_2 the perturbation around this prescribed flow ($\psi_i = \Psi_i - \overline{\Psi}_i$). The potential vorticity fields defined in Eqs. (3) and (4) can be written in terms of this perturbed streamfunction

$$q_1 = \nabla^2\psi_1 + \frac{\psi_2 - \psi_1}{\delta R^2} + \frac{U}{\delta R^2}\,y\,, \tag{7}$$

$$q_2 = \nabla^2\psi_2 + \frac{\psi_1 - \psi_2}{(1-\delta)\,R^2} - \frac{U}{(1-\delta)\,R^2}\,y. \tag{8}$$

We see that the prescribed eastward jet in the upper layer is associated with a meridional potential vorticity gradient (an "effective beta plane" term in the y direction) having an opposite sign in the upper and lower layers. The dynamics of the perturbation is then fully described by the potential vorticity advection,

$$\partial_t q_1 + J\left(\psi_1 - U\,y, q_1\right) = -A_h\nabla^6\psi_1, \tag{9}$$

$$\partial_t q_2 + J\left(\psi_2, q_2\right) = -A_h\nabla^6\psi_2 - r\nabla^2\psi_2. \tag{10}$$

When this equation is linearized around the prescribed eastward jet, we recover the Philipps model for baroclinic instability on a f-plane, see, e.g., Vallis.[3] In this configuration, the prescribed jet is always unstable and the most unstable mode is always associated with a horizontal scale that scales with the internal Rossby radius of deformation, whatever the value of bottom friction. Only the

time scale for the instability changes with bottom friction. Our aim is to study the non-linear equilibration of this instability. To trigger the baroclinic instability, we will consider an initial potential vorticity perturbation such that the corresponding perturbation velocity field is much smaller than the prescribed jet in the upper layer (velocity U). The initial condition for the potential vorticity fields q_1, q_2 is represented on Fig. 1(a), and this will be the same for all the numerical simulations presented in this paper.

It is worth noting that Eqs. (7)–(10) just describe the free decay of the total flow $(\psi_1 - U\,y, \psi_2)$ by the two layer quasi-geostrophic dynamics on a f-plane, in the presence of bottom friction and small scale dissipation. Note that since the perturbation is initially small, the total flow is initially the prescribed flow. In other words, the non-linear dynamics of a perturbation around a prescribed eastward jet in the upper layer is equivalent to a free decay experiment in which the initial condition would be given by the prescribed jet. We chose to decompose the total flow into a prescribed field $(\overline{\Psi}_1 = -U\,y, \overline{\Psi}_2 = 0)$, and an eddy field (ψ_1, ψ_2), because it allows to relate our results with previous studies performed in the context of doubly periodic geometry. Indeed, Eqs. (7)–(10) can be recast on the form

$$q_1' = \nabla^2\psi_1' + \frac{\psi_2' - \psi_1'}{\delta R^2}, \quad q_2' = \nabla^2\psi_2' + \frac{\psi_1' - \psi_2'}{(1-\delta)\,R^2}, \tag{11}$$

$$\partial_t q_1' + J\left(\psi_1', q_1'\right) = -U\partial_x q_1' - \frac{U}{\delta R^2}\partial_x\psi_1' - A_h\nabla^6\psi_1', \tag{12}$$

$$\partial_t q_2' + J\left(\psi_2', q_2'\right) = \frac{U}{(1-\delta)R^2}\partial_x\psi_2' - A_h\nabla^6\psi_2' - r\nabla^2\psi_2'. \tag{13}$$

Writing the dynamics in that way is convenient for simulations in the doubly periodic geometry since each field in this equation is doubly periodic. Because Eqs. (11)–(13) contain source and sinks terms on the right hand side, the non-linear dynamics of an initial perturbation around a prescribed baroclinically unstable flow is often referred to as forced-damped baroclinic turbulence. However, Eqs. (11)–(13) "hide" the conservative nature of the dynamics. It is clear from Eqs. (7)–(10) that this dynamics is actually a free decay dynamics, whatever the domain geometry. The only peculiarity of the doubly periodic geometry is that nontrivial statistical steady state may be reached in such freely decaying dynamics. We will see that transient states observed in the channel geometry are actually qualitatively similar to these statistical states of the doubly periodic geometry.

C. Conserved quantities

The flow model has a remarkable property: in the absence of small scale dissipation, the potential vorticity in the upper layer q_1 is advected without sinks nor sources. As a consequence, there are an infinite number of conserved quantities, namely, the Casimir functionals $\mathcal{C}_s[q_1] = \int_D \mathrm{d}x\mathrm{d}y\; s(q_1)$, where s is any sufficiently smooth function, see also Shepherd.[16] An equivalent statement is that the global distribution of the potential vorticity levels in the upper layer is conserved through the flow evolution when there is no small scale dissipation. Since the initial flow is characterized by $q_1|_{t=0} = U\,y/(\delta R^2)$, the global distribution of fine grained potential vorticity in the upper layer is a flat distribution of potential vorticity levels between $-UL_y/(2\delta R^2)$ and $UL_y/(2\delta R^2)$, see Fig. 1(b). Similarly, the global distribution of the potential vorticity in the lower layer is conserved if both the small scale dissipation and the bottom friction are zero. In that case, given our initial potential vorticity profile, the global distribution of potential vorticity levels in the lower layer is a flat distribution between $-UL_y/(2\delta R^2)$ and $UL_y/(2(1-\delta)R^2)$, see Fig. 1. If bottom friction is nonzero, the potential vorticity distribution of the lower layer is not conserved, but one may conjecture that the potential vorticity distribution of the lower layer remains bounded.[17] Remarkably, the presence of bottom friction does not affect conservation of the potential vorticity distribution in the upper layer.

When there is small scale dissipation, the global distribution of potential vorticity levels is no longer a conserved quantity. However, if the time scale for the relaxation of the initial condition towards a quasi-stationary state is smaller than the typical dissipation time scale, then one expects that the conservation laws of the inviscid dynamics still play an important role.

D. Energy budget

The energy of the perturbation is the sum of kinetic energy in each layer and of the available potential energy,

$$E = KE_1 + KE_2 + APE, \quad APE = \frac{1}{2}\int_{\mathcal{D}} \mathrm{d}x\mathrm{d}y \, \frac{(\psi_1 - \psi_2)^2}{R^2}, \tag{14}$$

$$KE_1 = \frac{\delta}{2}\int_{\mathcal{D}} \mathrm{d}x\mathrm{d}y \, (\nabla\psi_1)^2, \quad KE_2 = \frac{1-\delta}{2}\int_{\mathcal{D}} \mathrm{d}x\mathrm{d}y \, (\nabla\psi_2)^2. \tag{15}$$

In the absence of small scale dissipation, the temporal evolution of the energy of the perturbation is given by

$$\frac{R}{U}\frac{\mathrm{d}}{\mathrm{d}t}E = \frac{1}{R}\int_{\mathcal{D}} \mathrm{d}x\mathrm{d}y \, \psi_1\partial_x\psi_2 - (1-\delta)\frac{rR}{U}\int_{\mathcal{D}} \mathrm{d}x\mathrm{d}y \, (\nabla\psi_2)^2. \tag{16}$$

We readily note that the parameter rR/U plays a key role in the energy budget (16), and that this energy budget for the perturbed flow is the same as one would obtain in the doubly periodic geometry.[9] In the channel geometry, it is also useful to introduce the "total energy" defined as the energy of the flow that includes the perturbation and the prescribed eastward jet

$$E_{tot} = KE_{1tot} + KE_{2tot} + APE_{tot}, \quad APE_{tot} = \frac{1}{2}\int_{\mathcal{D}} \mathrm{d}x\mathrm{d}y \, \frac{(\psi_1 - Uy - \psi_2)^2}{R^2}, \tag{17}$$

$$KE_{1tot} = \frac{\delta}{2}\int_{\mathcal{D}} \mathrm{d}x\mathrm{d}y \, (\nabla(\psi_1 - Uy))^2, \quad KE_{2tot} = \frac{1-\delta}{2}\int_{\mathcal{D}} \mathrm{d}x\mathrm{d}y \, (\nabla\psi_2)^2. \tag{18}$$

The temporal evolution of the total energy is given by

$$\frac{\mathrm{d}}{\mathrm{d}t}E_{tot} = -(1-\delta)r\int_{\mathcal{D}} \mathrm{d}x\mathrm{d}y \, (\nabla\psi_2)^2. \tag{19}$$

This equation for the total energy allows for a clear physical interpretation in the channel case: in the presence of bottom friction, the total energy will decay to zero, provided that the kinetic energy of the bottom layer remains non-zero along the way. In other words, the perturbation will evolve toward the state $\psi_1 = Uy$, $\psi_2 = 0$ which annihilates the prescribed eastward flow U in the upper layer. We see from Eqs. (7) and (8) that such a state corresponds to fully homogenized potential vorticity fields $q_1 = q_2 = 0$. Note that this potential vorticity homogenization process does not rely on the existence of small scale dissipation, since the potential vorticity can be homogenized at a coarse grained level. The important mechanism is the filamentation process following sequences of stretching and folding of the potential vorticity field through turbulent stirring. If, for some reason, the kinetic energy of the lower layer vanishes at a given time ($\int_{\mathcal{D}} \mathrm{d}x\mathrm{d}y \, (\nabla\psi_2)^2 = 0$), then the system is trapped in a non-trivial steady state (as far as the energy budget is concerned). However, in all the simulations we performed, flows with $\psi_2 = 0$ and $r \neq 0$ were unstable, and solutions were therefore not attracted toward such states.

We will see in the following that the route towards complete potential vorticity homogenization strongly depends on the parameter rR/U. In particular, dimensional analysis predicts that the time scale for homogenization can be written in the general form

$$t_{diss} \sim \frac{1}{r}F_{diss}\left(\frac{rR}{U}, \frac{R}{L_y}, \delta, \frac{L_x}{L_y}\right), \tag{20}$$

where the arguments of the function F_{diss} are the four non-dimensional parameters of the problem, assuming vanishingly small scale dissipation ($A_h = 0$). We will argue in Sec. III that when the domain is large with respect to the Rossby radius of deformation ($L_y \gg R$), when the layer depth aspect ratio is of order one ($\delta \sim 1$), and when the domain aspect ratio is of order one ($L_x \sim L_y$), the function F_{diss} can be modeled by

$$F_{diss} = 1 + \left(\frac{rR}{U}\right)^2\frac{L_y}{R}. \tag{21}$$

For that purpose, we will need to discuss the vertical and the horizontal flow structures in the long time limit, before complete homogenization is achieved.

III. PREDICTIONS FOR THE FLOW STRUCTURE IN THE LONG TIME LIMIT

The aim of this section is to provide predictions for the vertical partition of the energy and to explore consequences of this vertical structure for the self-organization of the flow in the horizontal. We first show that barotropization is expected for vanishing bottom friction. We then explain that surface intensification is expected for large bottom friction. We then use a combination of arguments based on cascade phenomenology, potential vorticity homogenization theories, and equilibrium statistical mechanics in order to predict the horizontal flow structure in the large bottom friction limit and the small bottom friction limit. It is assumed in this section that the small scale dissipation is negligible ($A_h = 0$).

A. Barotropization in the low bottom friction limit

We consider first the case with zero bottom friction ($r = 0$). It will be useful to consider the barotropic and baroclinic modes of the two-layer model defined as

$$\psi_t = \delta\psi_1 + (1-\delta)\psi_2, \quad \psi_c = \psi_1 - \psi_2\,. \tag{22}$$

The baroclinic streamfunction ψ_c and the barotropic streamfunction ψ_t are related to the potential vorticity through

$$q_1 - q_2 = \nabla^2\psi_c - \frac{\psi_c}{\delta(1-\delta)R^2} + \frac{U}{\delta(1-\delta)R^2}\,y, \tag{23}$$

$$\delta q_1 + (1-\delta)q_2 = \nabla^2\psi_t. \tag{24}$$

The energy of the perturbation can be decomposed into a (purely kinetic) barotropic energy and a baroclinic energy that involves both kinetic energy and potential energy

$$E = KE_t + KE_c + APE_c, \quad APE_c = \frac{1}{2}\int_{\mathcal{D}} \mathrm{d}x\mathrm{d}y\,\frac{\psi_c^2}{R^2}. \tag{25}$$

$$KE_t = \frac{1}{2}\int_{\mathcal{D}} \mathrm{d}x\mathrm{d}y\,(\nabla\psi_t)^2, \quad KE_c = \delta\,(1-\delta)\,\frac{1}{2}\int_{\mathcal{D}} \mathrm{d}x\mathrm{d}y\,(\nabla\psi_c)^2. \tag{26}$$

Similarly, the total energy can be decomposed into a barotropic and a baroclinic component,

$$E = KE_{tot,t} + KE_{tot,c} + APE_{tot,c}, \quad APE_{tot,c} = \frac{1}{2}\int_{\mathcal{D}} \mathrm{d}x\mathrm{d}y\,\frac{(\psi_c - Uy)^2}{R^2}, \tag{27}$$

$$KE_{tot,t} = \frac{1}{2}\int_{\mathcal{D}} \mathrm{d}x\mathrm{d}y\,(\nabla(\psi_t - \delta U y))^2, \quad KE_{tot,c} = \delta\,(1-\delta)\,\frac{1}{2}\int_{\mathcal{D}} \mathrm{d}x\mathrm{d}y\,(\nabla\,(\psi_c - Uy))^2. \tag{28}$$

The initial potential vorticity fields in the upper and lower layers are $q_1^0 = Uy/\delta R^2$ and $q_2^0 = -Uy/(1-\delta)R^2$, respectively, plus a small perturbation. When $R \ll L_y$ and when $L_x \sim L_y$, the initial total energy is dominated by the potential energy: $E_{tot}^0 \sim APE_{tot}^0 \sim U^2L_y^4/R^2$.

The classical picture for two layer geostrophic turbulence predicts that the turbulent evolution of the flow leads to barotropization,[4–6] i.e., to a depth independent flow for which $E_{tot} \approx KE_{tot,t}$. In the context of freely evolving inviscid dynamics, the idea that barotropization may occur as a tendency to reach a statistical equilibrium state that takes into account dynamical invariants has been investigated by Refs. 18–20. It was found in these studies that barotropization may be prevented by conservation of potential vorticity levels in some cases. We provide in Appendix a phenomenological argument for barotropization in the case $R \ll L_y$, emphasizing the role of the conservation of potential vorticity levels, and of the total energy. In this limit, the flow dynamics is described at lowest order by the barotropic dynamics after its initial turbulent rearrangement,

$$\partial_t q_t + J(\psi_t, q_t) = 0, \quad q_t = \nabla^2\psi_t. \tag{29}$$

Let us now discuss the effect of a weak friction $rR/U \ll 1$. Let us call $t_{adv} = L_y/U$ the typical advection time scale for the flow over the whole domain. This can be considered as the typical time scale for the self-organization of the turbulent dynamics following the initial instability that occurs on a time scale $t_{inst} = R/U$. Once the flow is self-organized at the domain scale, if the flow is dominated by the barotropic mode, we see from Eq. (19) that the total energy should decay exponentially with an e-folding time $t_{diss} \sim 1/r$. This justifies the low friction limit for the function F_{diss} defined by Eq. (21).

B. Surface intensification in the large bottom friction limit

Whatever the bottom friction value, if the system reaches a quasi-stationary state, we see from energy budget equation (16) for the perturbed flow that the friction term $(1-\delta)(rR/U)\int_{\mathcal{D}} \mathrm{d}x\mathrm{d}y\ (\nabla\psi_2)^2$ must be of the order of the source term $(1/R)\int_{\mathcal{D}} \mathrm{d}x\mathrm{d}y\ \psi_1\partial_x\psi_2$. Let us now consider the large bottom friction limit, with a layer depth aspect ratio of order one ($\delta \sim 1$), a domain aspect ratio of order one ($L_x \sim L_y$), and a radius of deformation much smaller than the domain scale ($R \ll L_y$). Anticipating that typical horizontal scales of the flow structures will be in that case given by R, we find that typical variations of the stream function in the lower and the upper layers are related through

$$\psi_1 \sim \frac{rR}{U}\psi_2. \tag{30}$$

We conclude that $\psi_1 \gg \psi_2$ when $rR/U \gg 1$. At lowest order, only the upper layer is active and the flow can be described by a $1^1/_2$ layer quasi-geostrophic model

$$\partial_t q_1 + J(\Psi_1, q_1) = 0, \tag{31}$$

with the notation $\Psi_1 = \psi_1 - U\,y$ and with

$$q_1 = \nabla^2\Psi_1 - \frac{\Psi_1}{\delta R^2}. \tag{32}$$

Let us now estimate the typical time scale for the energy evolution. Anticipating the emergence of ribbons, we assume that the total energy is dominated by the potential energy $E_{tot} \sim L_y^2\Psi_1^2/R^2$. This energy should decay with time according to Eq. (19). We use scaling equation (30) to estimate $\int_{\mathcal{D}} \mathrm{d}x\mathrm{d}y(\nabla\psi_2)^2 \sim U^2\psi_1^2 L_y/(r^2R^3)$. Introducing the dissipation time t_{diss} such that $dE_{tot}/dt \sim E_{tot}/t_{diss}$ and assuming $\psi_1 \sim \Psi_1$, we get

$$t_{diss} \sim \frac{1}{r}\left(\frac{rR}{U}\right)^2\frac{L_y}{R}. \tag{33}$$

This leads to a surprising result: in the large bottom friction limit, the typical time scale for the evolution of the quasi-stationary large scale flow is proportional to the bottom friction coefficient. In other words, dissipation time increases with the friction. This estimate for the dissipation time in Eq. (33) justifies our choice for F_{diss} in Eq. (21) in the limit $rR/U \gg 1$ and $\delta^{1/2}R \ll L_y$. The main caveat of this argument is the assumption that $\psi_1 \sim \Psi_1$ which cannot be valid at short time (when the instability grows) and in the long time limit (when the perturbation has almost annihilated the prescribed eastward jet). However, we will show that this provides a reasonable scaling to interpret the numerical simulations. In addition, the same argument applied to the energy budget of perturbed flow equation (19), without assuming $\psi_1 \sim \Psi_1$, would show that t_{diss} is the typical time scale for the growth of the potential energy of the perturbed state.

As far as friction is concerned, the behaviour of the system is analogous to a damped oscillator described by the dynamical equation $m\ddot{x} - r\dot{x} + kx = 0$. In the low friction limit, the time scale for energy dissipation is simply $1/r$. In the large friction limit, the time scale for energy dissipation is r/k: dissipation time increases linearly with friction coefficient in the overdamped limit.

C. Cascade phenomenology for quasi-geostrophic models

The flow in the large friction limit $rR/U \gg 1$ and in the low friction limit $rR/U \ll 1$ is both described at lowest order by a one layer flow model

$$\partial_t q + J(\psi, q) = 0, \quad q = \nabla^2\psi - \lambda_d^{-2}\psi. \tag{34}$$

We recover barotropic dynamics equation (29) when $\lambda_d = +\infty$ and $1\frac{1}{2}$ layer quasi-geostrophic dynamics equations (31) and (32) when $\lambda_d = \delta^{1/2}R$.

We consider Eq. (34) with an arbitrary λ_d and we introduce the relative vorticity $\zeta = \nabla^2\psi$. At spatial scales much smaller than λ_d, the potential vorticity q is dominated by the relative vorticity and the dynamics is given by the 2D Euler equation

$$\partial_t \zeta + J(\psi, \zeta) = 0. \tag{35}$$

Classical arguments[21,22] predict a direct cascade of enstrophy $Z = \int_{\mathcal{D}} \mathrm{d}x\mathrm{d}y\ \zeta^2/2$ and an inverse cascade of kinetic energy $E_{kin} = -\int_{\mathcal{D}} \mathrm{d}x\mathrm{d}y\ \psi\zeta/2$. In the freely evolving case, one expects a decrease of the kinetic energy k-centroid $k_{E_{kin}} = \int \mathrm{d}k\ k\mathcal{E}_{kin}(k)/E_{kin}$ until the energy is condensed at the domain scale, and a concomitant increase of the enstrophy k-centroid $k_Z = \int \mathrm{d}k\ k\mathcal{Z}(k)/Z$, where $\mathcal{E}_{kin}(k)$ and $\mathcal{Z}(k)$ are the kinetic energy and enstrophy spectra.[23]

At spatial scales much larger than λ_d, dynamics equation (34) is the so-called planetary geostrophic model[24]

$$\partial_\tau \psi + J(\zeta, \psi) = 0, \tag{36}$$

with $\tau = \delta R^2 t$. The role of ζ and ψ are switched with respect to the Euler dynamics. The same arguments used in the Euler case predict now a direct cascade of kinetic energy E_{kin} and an inverse cascade of potential energy[25,26] $E_p = \int_{\mathcal{D}} \mathrm{d}x\mathrm{d}y\ \psi^2/(2\lambda_d^2)$. In the freely evolving case, one expects that the potential energy centroid will go to large scale until condensation at the domain scale. Meanwhile, the kinetic energy centroid should go to small scales.

We see that in both in the small scale limit described by Eq. (35) and in the large scale limit described Eq. (36), the kinetic energy is expected to pile up at scale $\lambda_d = \delta^{1/2}R$.

We also note that the concomitant condensation of potential energy at the domain scale with a direct cascade of kinetic energy (halted around the scale $\delta^{1/2}R$) is necessarily associated with the formation of large regions of homogenized streamfunction at a coarse grained level (or equivalently homogenized potential vorticity). In other words, the streamfunction gradients are expelled at the boundary between regions of homogenized potential vorticity. This justifies with a dynamical point of view the emergence of ribbons. Another complementary point of view is to say that the dynamics tends to homogenize the potential vorticity field, but that a complete homogenization would not be possible due to energy conservation. In the limit $\delta^{1/2}R \ll L_y$, the dynamics will therefore tend to form at least two regions of homogenized potential vorticity at the domain scale, which allows a sustained large scale available potential vorticity field, while allowing for potential vorticity homogenization almost everywhere.

Let us now come back to the problem of the non-linear equilibration of a baroclinically unstable eastward jet in the large bottom friction limit. We explained in Subsection III B that the dynamics is given in that case at lowest order by $1\frac{1}{2}$ layer quasi-geostrophic dynamics, and we saw in this subsection that this should lead to the formation of homogenized regions of potential vorticity. Typical values of the upper layer potential vorticity in the region where it is homogenized can be estimated as $\mathcal{Q}_1 \sim UL/\delta R^2$, assuming that the total energy of the flow presenting two regions of homogenized regions of potential vorticity is of the order of the initial energy of the baroclinically unstable eastward jet. We see from (32) that sufficiently far from the interface, between two regions of homogenized potential vorticity, the streamfunction is also a constant with $\Psi_1 \sim \delta R^2 \mathcal{Q}_1 \sim UL_y$. The interfaces between different regions of homogenized potential vorticity correspond therefore to jumps of the streamfunction, which occur at a typical scale $\delta^{1/2}R$. This corresponds to strong localized jets with velocity $V \sim \Psi_1/(\delta^{1/2}R) \sim UL_y/(\delta^{1/2}R)$. The length of these jets is of order of the domain size L_y, much larger than their width, of order $\delta^{1/2}R$, hence the term "ribbons." The fact that potential vorticity fronts lead to much sharper jets in $1\frac{1}{2}$ layer flows than in barotropic one layer flows has been emphasized previously by Arbic and Flierl,[9] Bouchet and Sommeria.[12]

To conclude, the flow should self-organize into a large scale structure with velocity variations at the scale of the domain L_y in the low bottom friction limit $rR/U \ll 1$ and form ribbons of width $\delta^{1/2}R$ and length L_y in the large bottom friction limit $rR/U \gg 1$. More detailed predictions for the large scale flow structure can be obtained in the framework of equilibrium statistical mechanics, as discussed in Subsection III D.

D. Statistical mechanics predictions for the large scale flow structure

Turbulent dynamics stretches and folds potential vorticity filaments which thus cascade towards smaller and smaller scales. This stirring tends to mix the potential vorticity field at a coarse-grained level, even in the absence of small scale dissipation. If there is no energy constraint and if there is enough stirring, the potential vorticity field should be fully homogenized just as in the case of a passive tracer. By contrast, complete homogenization cannot be achieved if there is an energy constraint, which leads to nontrivial large scale flow structures, and statistical mechanics gives a prediction for such large scale flows. The aim of this subsection is to review existing results on the statistical mechanics theory for one layer quasi-geostrophic models that will be useful to interpret our numerical results.

1. Miller-Robert-Sommeria (MRS) theory for a barotropic model

The theory was initially developed by Robert and Sommeria,[11] Miller, Weichman, and Cross,[27] and will be referred to as the MRS theory in the following. We provide here a short and informal presentation of this approach—see also reviews by Refs. 28–31.

The theory provides a variational problem that allows computation of the most probable outcome of turbulent stirring at a macroscopic (or coarse-grained) level among all the microscopic configurations of the flow that satisfy the constraints of the dynamics given by the conservation of the energy and of the global distribution of potential vorticity levels. Large deviation theory shows that an overwhelming number of microscopic states correspond to the most probable macroscopic state. The only assumption is ergodicity, i.e., that there is sufficient mixing in phase space for the system to explore all the possible configurations given the dynamics constraints.

In the case of a one layer quasi-geostrophic flow described by Eq. (34), the input of the theory is given by the energy of the flow E and the initial fine-grained (or microscopic) potential vorticity distribution $\gamma(\sigma)$. The output of the theory is a field $p(x, y, \sigma)$ that gives the probability density function to measure a potential vorticity level $\sigma \in \Sigma$ in the vicinity of the point (x, y). This field defines a macroscopic state of the system, which allows us to keep track of the dynamical constraints. The computation of the equilibrium state amounts find the field p that maximizes a mixing entropy $\mathcal{S} = -\int_\Sigma \mathrm{d}\sigma \int_\mathcal{D} \mathrm{d}x\mathrm{d}y\ p \ln p$ with the constraints given by dynamical invariants expressed in term of p. This entropy counts the number of micro states associated with a given macro state p.[11,27] The constraints are given by the conservation of the global distribution $\gamma(\sigma) = d_\sigma$ with $d_\sigma[p] = \int_\mathcal{D} \mathrm{d}x\mathrm{d}y \int \mathrm{d}\sigma p$ and the energy conservation $E = \mathcal{E}[p]$ with $\mathcal{E}[p] = -\int_\mathcal{D} \mathrm{d}x\mathrm{d}y \int \mathrm{d}\sigma\sigma p\psi$. Note that the energy constraint is obtained by assuming that the energy of local vorticity fluctuations is negligible. The validity of this mean-field treatment can be proven using large deviation theory. The potential vorticity field of the equilibrium state is $\overline{q} = \int_\Sigma \mathrm{d}\sigma\ \sigma p$, and the streamfunction is obtained by inverting $\overline{q} = \nabla^2\psi - \lambda_d^{-2}\psi$. We stress that the theory applies for flows without small scale dissipation. In the presence of small scale dissipation, the predictions of the theory are expected to be valid only if the typical time scale for self organization of the flow is much smaller than the typical time associated with small scale dissipation. We also note that in that case, once the flow is self-organized, small scale dissipation smears out local fluctuations of the potential vorticity field so that the microscopic potential vorticity field q actually tends to the macroscopic field $\overline{q}$.

The equilibrium state is always characterized by a monotonic functional relation $\overline{q} = g(\psi)$.[11,27] This function g depends only on the dynamical invariants. At this stage two approaches could be followed. A first approach is to consider E and $g(\sigma)$ as given, to compute the function g, and the flow structure associated with the corresponding equilibrium state. A second approach is to assume a given $q - \psi$ relation and to compute the MRS statistical equilibria associated with this relation.

This second approach has made possible several analytical results in the last decade, and we will rely on these results to interpret our simulations.

Although computation of the equilibrium state is a difficult task in general, several analytical results can be obtained in limiting cases[30] for a detailed discussion. For instance, whatever the initial distribution of potential vorticity levels, it can be shown that low energy states are always characterized at lowest order by a linear $q - \psi$ relationship, whose coefficient only depend on the total energy, the total enstrophy, and the circulation.[30] Here, low energy means that the energy of the flow is much smaller than the maximum admissible energy for a given potential vorticity distribution. In our case, the initial total energy is of the order of $U^2 L_y^3 L_x / R^2$. It is not difficult to construct a state, with the same global distribution of potential vorticity levels, that is characterized by an energy that scales as $U^2 L_y^3 L_x / R^4$, which is therefore much larger than the initial energy provided that $\delta^{1/2} R \ll L_y$. This justifies the low energy limit for the weak friction case.

Such a low energy limit allows us to compute analytically phase diagrams for the flow structure and to describe how this flow structure changes when the energy or the enstrophy of the flow is varied. For instance, statistical equilibria associated with a linear $q - \psi$ relation have been classified for various flow models in an arbitrary closed domain[32,33] and on a channel.[34] In particular, it was shown in these studies that when the flow domain is sufficiently stretched in the x direction, then the equilibrium state is a dipolar flow.

2. Application to the 1½ layer quasi-geostrophic model

In the large friction limit $rR/U \gg 1$, our justification for the relevance of the "low energy limit" of Subsection III D 1 is no more valid. Indeed, this justification relied on the estimates for the energy provided in Appendix, assuming that the flow is fully barotropic. Yet we have shown previously that in the large friction limit, the flow is not barotropic but is described at lowest order by 1½ quasi-geostrophic dynamics equation (34) with $\lambda_d = \delta^{1/2} R$. When $\delta^{1/2} R \ll L_y$, i.e., when the Rossby radius of the upper layer is much smaller than the domain scale, it has been shown by Bouchet and Sommeria[12] that a class of equilibrium states different than the low energy states of Sec. III D 1 can be computed analytically. Assuming that the $q - \psi$ relation is tanh-like, they showed that the equilibrium state is composed of two subdomains with homogenized potential vorticity separated by jets of width $\delta^{1/2} R$ at their interface, see also Weichman,[35] Venaille and Bouchet.[36] Statistical mechanics also predicts in that case that the interface between the two regions of homogenized potential vorticity should be minimal, just as bubbles in usual thermodynamics. A key assumption for these results is that the $q - \psi$ relation of the equilibrium state has a tanh-like shape. In the case of an initial distribution $\gamma(\sigma)$ with only two levels of potential vorticity, it can be shown than the $q - \psi$ relation is given exactly by a tanh function.[12] Bouchet and Sommeria[12] conjectured that there exists a much larger class of initial energy E and of fine-grained potential vorticity distributions $\gamma(\sigma)$ that leads to a tanh-like shape for the $q - \psi$ relation at equilibrium. Our phenomenological arguments above and our numerical results below suggest that the dynamics is indeed attracted toward a quasi-stationary state characterized by such a tanh-like relation in a case where the initial distribution of potential vorticity levels is far from a double delta function, see Fig. 1.

IV. NUMERICAL RESULTS

A. Numerical settings

Quasi-geostrophic simulations are performed using the same numerical model as in Nadeau and Straub.[37] No normal flow and slip conditions are imposed at lateral walls. We use a third order Adams-Bashforth scheme for time derivatives, center differencing in space, an Arakawa scheme for the Jacobian,[38] and a multigrid method for the elliptic inversions. Momentum conservation is achieved following a procedure similar to that of McWilliams, Holland, and Chow,[14] using the zonal momentum equation integrated over a latitude circle in the channel.

To trigger the baroclinic instability, we considered an initial potential vorticity perturbation such that the corresponding velocity field was characterized by random phases and a gaussian spectrum of width $\Delta k = 2$ and peaked at $k = 6$; the perturbations were such that $\Psi_1^{init} k \ll U$. As we will see in the high bottom friction limit, the dynamics required thousands of eddy turn-overtimes, hence the moderate horizontal resolution. This initial condition is the same for all the numerical simulations presented in the paper, and the corresponding potential vorticity fields q_1, q_2 are represented on Fig. 1.

There are five adimensionalized parameters in this problem: the adimensionalized bottom friction coefficient rR/U, the aspect ratio L_x/L_y, the adimensionalized internal Rossby radius of deformation R/L_y, the ratio δ of the upper layer depth with the total depth, and the Reynolds number based on the small scale dissipation coefficient A_h. The small scale dissipation coefficient is adjusted to the lowest necessary value to ensure convergence of the simulation for a given resolution. Arbic and Flierl[9] did show that the results of such simulations do not depend strongly (at least qualitatively) on the form chosen for the small scale dissipation term. We also checked that our results were not dependent on the chosen resolution. Consistent with the exponential stratification observed in most parts of the oceans, we consider that the upper layer is thin compared to the lower layer, with $\delta = 0.2$, and this parameter will be constant for all the simulations. This choice is also reasonable to test the scaling predictions obtained for $\delta \sim 1$. There remain three parameters. The main control parameter is rR/U which is varied from 0 to 40, in order to test our scaling predictions obtained for $rR/U \ll 1$ and $rR/U \gg 1$. We considered a ratio $R/L_y = 0.1$ for the reference case (which corresponds to $\delta^{1/2} R/L_y = 0.004$) but also looked at the effect of decreasing this parameter. In any case, this parameter can be considered to be much smaller than one. We finally considered the aspect ratio $L_x/L_y = 5/3$ for the reference case, which corresponds to a 897 by 513 grid in physical space. We explored the effect of varying the domain aspect ratio, but always in the regime $L_y \sim L_x$. These parameters are summarized in Table I.

B. The role of bottom friction

1. Energy decay and potential vorticity homogenization

We first discuss reference simulations for which the aspect ratio is $L_x/L_y = 5/3$ and the Rossby radius is $R/L_y = 0.1$. We present in Fig. 2 the temporal evolution of the total kinetic energy $KE_{tot} = KE_{1tot} + KE_{2tot}$ and of the total available potential energy APE_{tot} defined in Eq. (18), for various values of the bottom friction coefficient rR/U. We see that in any case, the total available potential energy APE_{tot} decreases and eventually vanishes. We distinguish three regimes for the temporal evolution of the kinetic energy KE_{tot},

1. the initial growth of KE_{tot},
2. the saturation regime where KE_{tot} reaches its maximal value,
3. the decay of KE_{tot} due to bottom friction (except when $rR/U = 0$).

TABLE I. Model parameters for the reference simulations. Other simulations have been performed by varying R/L_y and Lx/L_y.

Parameter	Value
Imposed velocity	$U = 1$ m s^{-1}
Channel width	$L_y = 900$ km
Fractional depth of the upper layer	$\delta = 0.2$
Rossby radius	$R/L_y = 0.1$
Channel aspect ratio	$L_x/L_y = 5/3$
Bottom friction coefficient	rU/R from 0 to 40
Horizontal resolution	$\Delta x = \Delta y = 1.7$ km
Bi-harmonic dissipation coefficient	$A_h = 1 \times 10^8$ s^{-1}m^4

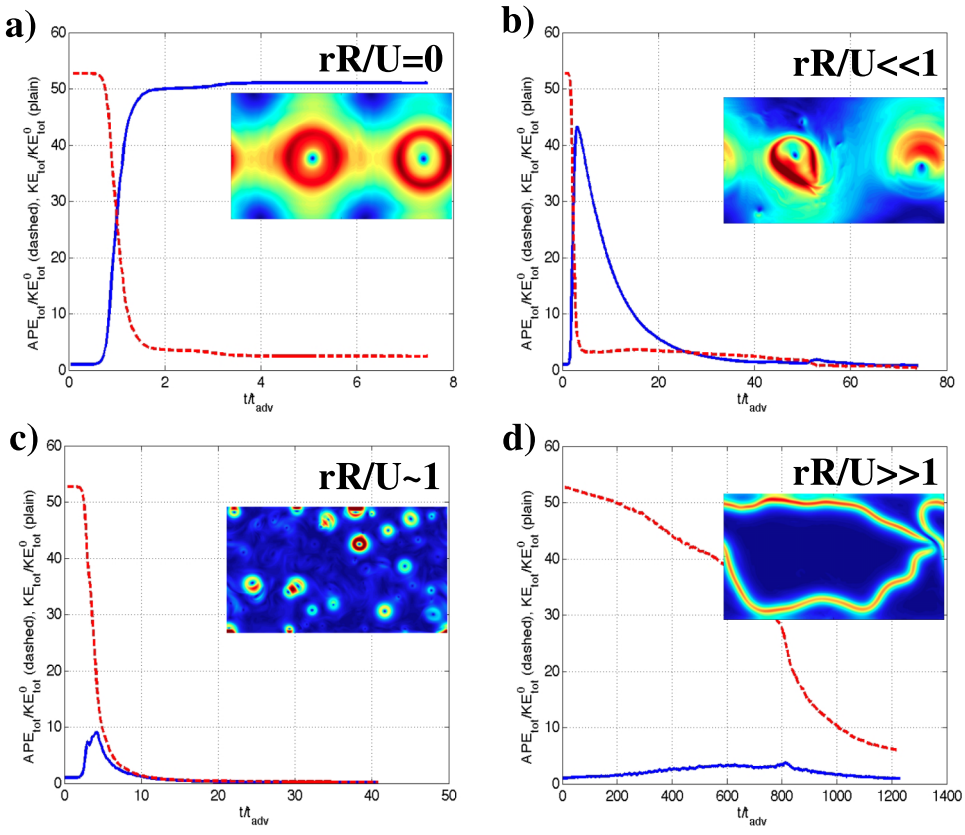

FIG. 2. (a) Temporal evolution of the total kinetic energy KE_{tot} and of the total potential energy APE_{tot} in the case $rR/U = 0$. Time is normalized by $t_{adv} = L_y/U$. The energy values on y-axis are normalized by the initial total kinetic energy. The field in inset represents a snapshot of the velocity modulus during the kinetic energy decay. (b) *Idem* $rR/U = 0.004$. (c) *Idem* for $rR/U = 0.5$. (d) *Idem* for $rR/U = 40$. Note that the flow structures in each regime are similar to Fig. 7 of Arbic and Flierl.[9]

As explained before, the decay of the total energy to zero indicates the potential vorticity field is fully homogenized, so that the perturbation has cancelled the effect of the prescribed eastward jet. Remarkably, the different routes towards complete homogenization and the time scales associated with it are completely different depending on the value of rR/U, which appears clearly on the temporal evolution of the global distribution of potential vorticity levels in the upper layer, see Fig. 3. The observed flow structures during this energy decay also strongly depend on the coefficients rR/U as shown on the insets of Fig. 2. In the weak friction case, the flow is a large scale dipolar vortex condensed at the domain scale. In the large bottom friction limit, the flow is a ribbon of kinetic energy of width given by $\delta^{1/2}R$, and in the intermediate bottom friction limit, the flow is made of isolated vortices whose size is of the order of the Rossby radius of deformation R. We note that all these flow configurations are qualitatively similar to those reported in the doubly periodic geometry by Arbic and Flierl.[9]

2. Estimate for the dissipation time

We compare on Fig. 4(a) the temporal evolution of the total kinetic energy KE_{tot} for various values of rR/U. Clearly, the time scales for this temporal evolution strongly depend on the value of rR/U. Let us first discuss the initial energy growth. It is a classical result that in the weak friction regime $rR/U \ll 1$ the typical time for baroclinic instability scales as R/U, hence the initial collapse of all the curves that belong to this regime on Fig. 4(a). For the same reason, the saturation of the instability due to self-organization following turbulent stirring always occurs at a time scale of

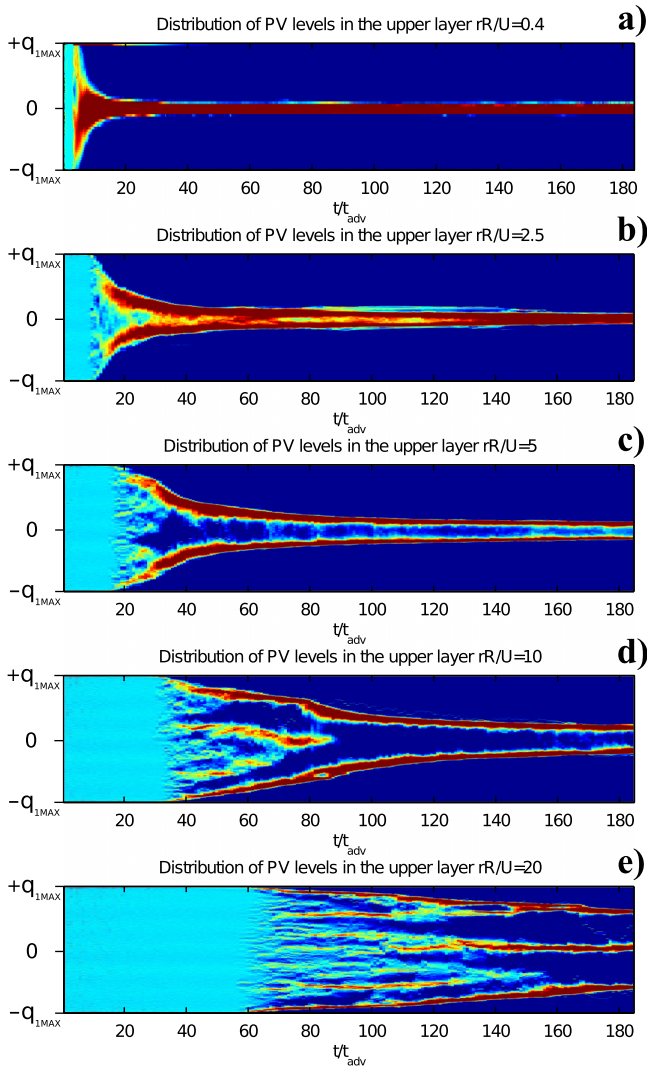

FIG. 3. Routes towards potential vorticity homogenization depending on bottom friction. Each panel represents the temporal evolution of the global distribution of potential vorticity levels in the upper layer. Time is adimensionalized by $t_{adv} = U/L_y$.

the order of the advection time $t_{adv} = L_y/U$ in this low friction regime. By contrast, in the high friction limit $rR/U \gg 1$, a direct computation of the linear baroclinic instability would show that this instability increases linearly with the bottom friction coefficient r. In addition, our estimate for the non-linear growth of the energy of the perturbation (see the end of Subsection III B) leads to a time t_{diss} that also scales linearly with the bottom friction coefficient r. These predictions agree qualitatively with the fact that kinetic energy peaks occur at larger time with increasing bottom friction coefficient r on Fig. 4(a).

We focus now on the kinetic energy decay. For a given value of the parameter rR/U, we estimate on Fig. 4(b) the decay time t_{diss} as the time interval between the kinetic energy maximum KE_{max} and $KE_{max}/4$. We see that the predictions for this dissipation time given by Eqs. (20) and (21) yield a good qualitative understanding of the numerical simulations in the low bottom friction regime ($t_{diss} \sim 1/r$) and the large bottom friction regime ($t_{diss} \sim r$). In order to test in more detail these predictions for the energy dissipation time scale, we plot on Fig. 4(c) the temporal evolution of the kinetic energy starting from t_{max}, the time when the maximum total kinetic energy has been reached, by renormalizing time with the dissipation time t_{diss} given by Eqs. (20) and (21), for each of the rR/U values. Remarkably, and despite the four decades range for rU/R, all the curves for the

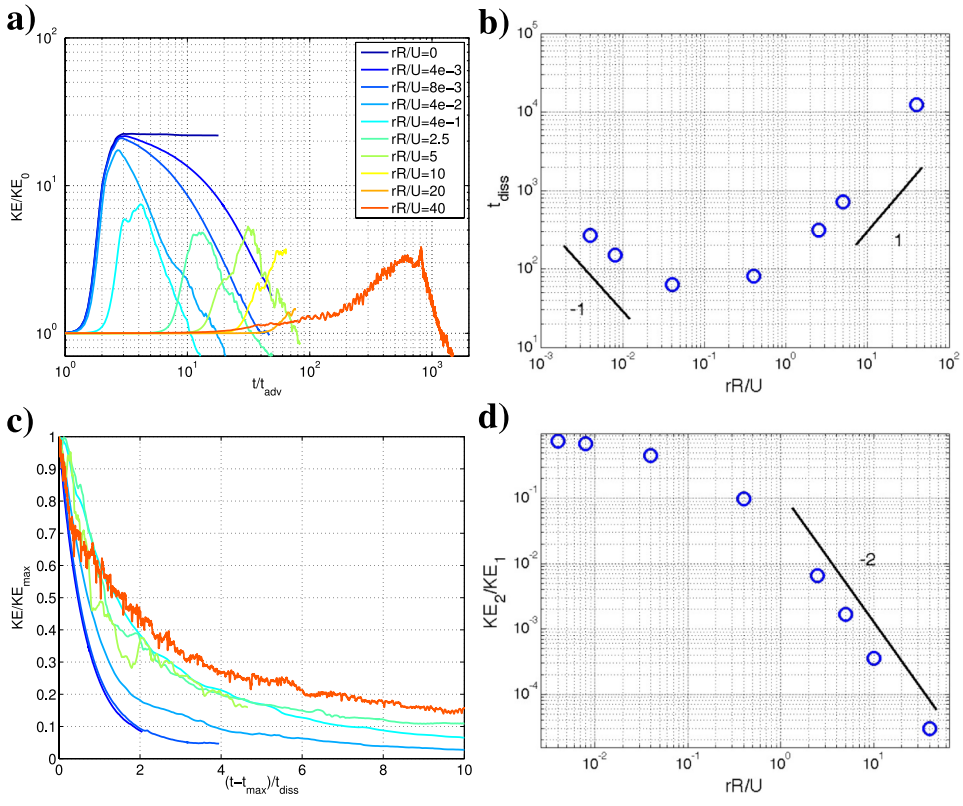

FIG. 4. (a) Temporal evolution of the total kinetic energy $KE = KE_1 + KE_2$. The kinetic energy is normalized by its initial value, and the time scale is normalized by the advection time $t_{adv} = L_y/U$. The logarithm scale is used in order to see all the runs on the same plot. (b) Estimation of the dissipation time in the numerical experiment (see text for details). (c) Temporal decay of the kinetic energy KE_{tot}. The time series are the same as on panel (a), but KE_{tot} is normalized for each run by its maximum value, the time coordinate is normalized by the dissipation time defined in Eqs. (20) and (21), and the time origin has been translated for each run so that $t = 0$ corresponds to the time where the kinetic energy is maximal. (d) Ratio of the kinetic energy in the upper and the lower layers for different values of the parameter rR/U (this ratio is computed for quasi-stationary states in the long time limit).

energy decay collapse reasonably well. This collapse confirms not only that the scaling obtained in the limiting cases are correct but also that the prefactors are qualitatively correct.

3. Vertical flow structure

We show on Fig. 4(d) the ratio $\delta KE_{2tot}/(1-\delta)KE_{1tot}$ of the total kinetic energy in each layer normalized by the depth of these layers, as a function of the parameter rR/U. We expect from Subsection III A that this energy ratio tends to one when $rR/U \ll 1$, i.e., that the flow has become barotropic. We expect from scaling equation (30) that this energy ratio should scale as $\sim (rR/U)^{-2}$ for large rR/U. We see a very good agreement between these predictions and our numerical results on Fig. 4(d). We stress that both scalings are based on the fact that the flow is self-organized into a quasi-stationary state. This contrasts with the scaling $\delta KE_{2tot}/(1-\delta)KE_{1tot} \sim (rR/U)^{-4/3}$ proposed by Arbic and Flierl[9] by revisiting a cascade argument by Held and Larichev.[39] We believe that their scaling is relevant to describe the vertical structure of the flow for $rR/U \gg 1$ provided that the potential energy length scale remains smaller than the domain size. Since the potential energy length scale increases with rR/U, this scaling should break at some point. In any case, both our scaling and the scaling of Arbic and Flierl[9] predict that the dynamics is well described by a $1^1/_2$ quasi-geostrophic model in the limit of large frictions $rR/U \gg 1$ and by a barotropic flow model in the low friction limit $rR/U \ll 1$. The next two subsections are devoted to the description of the flow structure in both regimes.

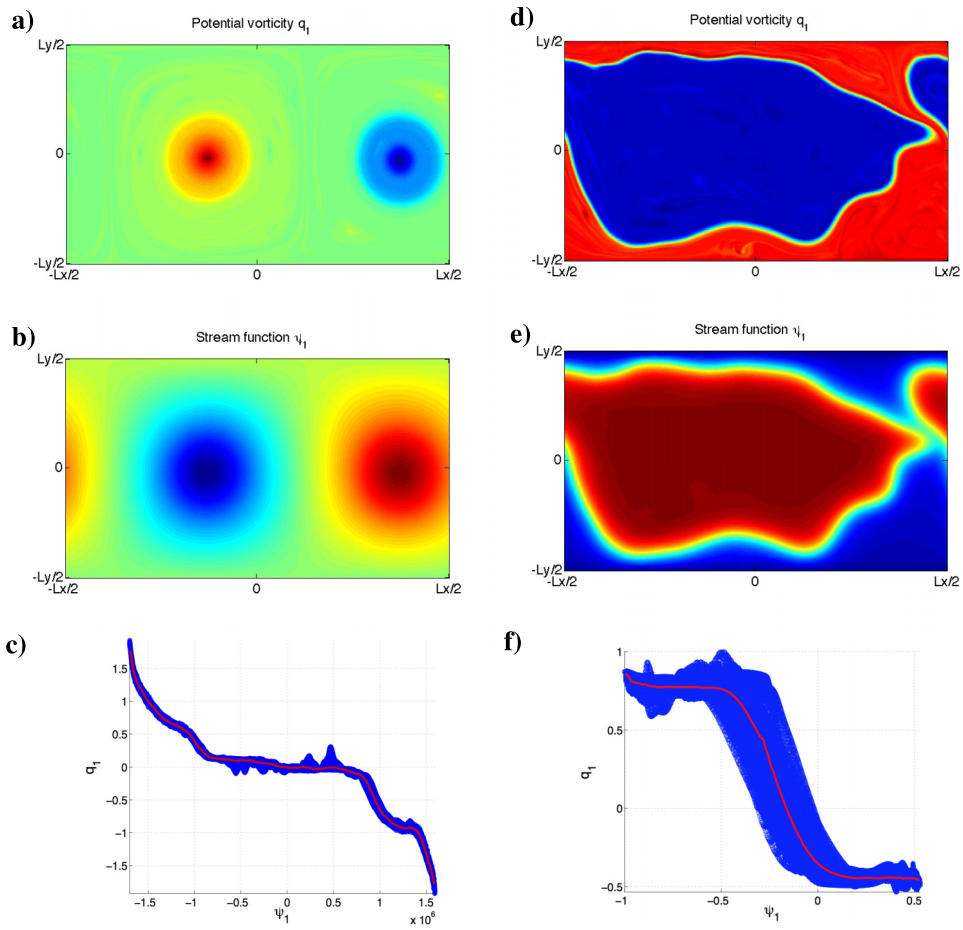

FIG. 5. (a) Representative late time snapshot of the potential vorticity field in the upper layer for $rR/U = 0$. (b) Corresponding streamfunction field in the upper layer (c) scatterplot of the $q - \psi$ relation associated with a and b. (d), (e), and (f) Same plots in the case with large bottom friction $rR/U \ll 1$.

C. Weak friction limit

We see in Fig. 2(a) that the flow reaches a stationary state when $rR/U = 0$. We checked that in this state, 80% of the kinetic energy was in the barotropic mode, which is in agreement with the fact that barotropization is expected with corrections of order δ or R/L_y when $rR/U \ll 1$ and $\delta \ll 1$, see the discussion in Subsection III A. We also note that the initial potential energy reservoir of the baroclinically unstable eastward jet ($APE^0_{tot} \gg KE^0_{tot}$) has been transferred almost totally into kinetic energy, due to the conservation of the total energy $E_{tot} = APE_{tot} + KE_{tot}$. We see in Figs. 5(a) and 5(b) that the corresponding large scale streamfunction and potential vorticity fields are self-organized into a dipolar structure at the domain scale. This dipole is characterized by a monotonic relation between potential vorticity and streamfunction. This functional relation has roughly a sinh shape. This sinh shape is different than the linear $q - \psi$ relation that one would expect in a low energy limit for an initial prescribed potential vorticity distribution. We explained in Subsection III D 1 that the total energy in the numerical experiment is much smaller than the maximal admissible energy with the same initial global distribution of potential vorticity levels. The reason why a linear $q - \psi$ relation is not observed here is that the core of the remaining vortices has not been stirred during the turbulent evolution of the flow. This shows a lack of ergodicity for the dynamics, which has been discussed for instance by Schecter *et al.*[40] However, we note that the observed dipolar structure is the flow that would be predicted by the MRS theory applied to the barotropic model in a channel sufficiently stretched in the x-direction, as explained in Subsection III D 1.

In the presence of a weak bottom friction ($rR/U \ll 1$), the large scale state becomes quasi-stationary and the total kinetic energy decreases with a time scale of the order of $1/r$ until the total energy vanishes. By quasi-stationary we mean that there still exists a well defined $q - \psi$ relation, but with superimposed small fluctuations that increase when bottom friction increases. The total energy decay goes with the homogenization of the potential vorticity fields. This route towards potential vorticity homogenization is illustrated in Fig. 3(a). We see on this figure the rapid emergence of one broad central peak for the global potential vorticity distribution, which indicates that the background potential vorticity field is well mixed over a time $t_{adv} \sim L_y/U$, and the width of the peak decreases more slowly, over a time scale of the order of $1/r$. We also remark that two isolated peaks with large potential vorticity values persist until $t_{diss} \sim 1/r$. These peaks correspond to the unmixed core of the dipolar structure. The increase of their strength is an artifact due to the use of a biharmonic dissipation operator. This would not occur with viscous dissipation.

We note that this route towards complete potential vorticity homogenization and dissipation of the energy of the initial baroclinically unstable eastward jet is very much like the classical scenario for two-layer baroclinic turbulence: the instability leads to an inverse energy cascade in the horizontal, with barotropization in the vertical, and then bottom friction dissipates the energy of the large scale flow.[5,6]

When the bottom friction is further increased, the inverse energy cascade is arrested before the flow self-organizes at the domain scale, and the number of vortices increases. When rR/U is of order one, the bottom friction time scale $\sim 1/r$ is of the order of the linear baroclinic instability time scale R/U. One expects therefore that flow structures cannot grow larger than the scale of injection, which is the scale of the most unstable mode for linear instability and secondary instabilities, of order R. This explains the formation of coherent structures of size R on Fig. 2(c). These eddies rapidly mix the background potential vorticity field, on the advection time scale $t_{adv} = L_y/U$, as seen on Fig. 3(b). This is a strongly out-of-equilibrium regime that cannot be described by MRS equilibria. In the doubly periodic geometry, this regime of vortex kinetics can be statistically steady and has been studied in detail by Thompson and Young.[7] In the case of the channel, the number of isolated vortices decreases with time until the potential vorticity field is fully homogenized.

D. Large friction limit

1. Emergence of the ribbons

A typical snapshot of the potential vorticity field when a quasi-stationary state is reached is presented in Fig. 5(d) for the case $rR/U = 40$. Clearly, at sufficiently large time, the flow has reached a state characterized by two regions of homogenized potential vorticity separated by a sharp interface. By sharp we mean that the interface between the homogenized regions is much smaller than the Rossby radius of deformation of the upper layer $\delta^{1/2}R$. This sharp interface in the potential vorticity field induces typical variations of streamfunction at scale $\delta^{1/2}R$ in the transverse direction, see Fig. 5(e). The scatterplot of the potential vorticity field and streamfunction field is plotted on Fig. 5(f) and shows a tanh-like shape for the $q_1 - \psi_1$ relation. The red line is the averaged potential vorticity along one streamline. The presence of fluctuations around this red line indicates that contrary to the case $rR/U = 0$, the large scale flow is not exactly a stationary state: the interface meanders intermittently break, and the blobs of potential vorticity exchanged during these breaking events are then stretched and folded in each region of homogenized potential vorticity, hence the presence of potential vorticity fluctuations.

It is notable that the dynamics drives the system towards a state characterized by a "tanh" relation between vorticity and streamfunction, given that the initial potential vorticity field in the upper layer is a gradient in the meridional direction presenting no region of homogenized potential vorticity. In that respect, our results support for the claim of Bouchet and Sommeria[12] that phase separation of the potential vorticity field into two homogenized regions is a generic feature of $1^1/_2$ layer quasi-geostrophic equilibria, that does not depend on the particular initial condition when $\delta^{1/2}R/L_y \ll 1$.

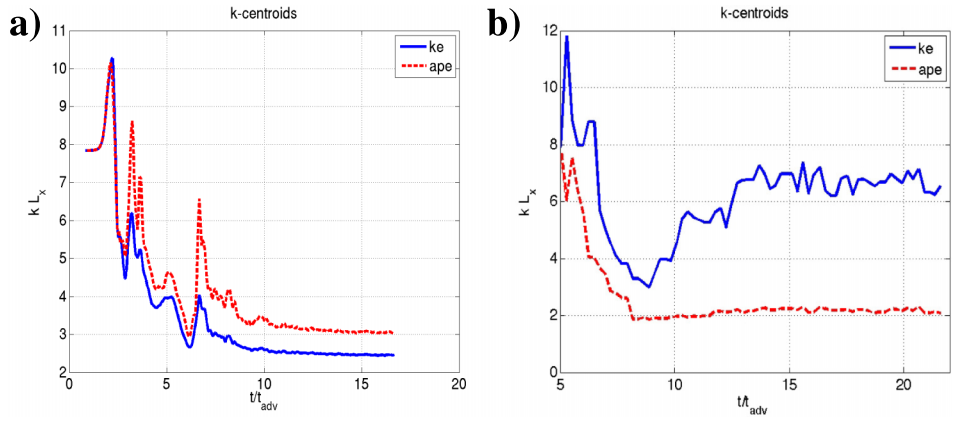

FIG. 6. (a) Initial temporal evolution of the barotropic kinetic energy k-centroid $k_{KE_t} = \int dk\ k\widetilde{KE}_t(k)/\int dk\ \widetilde{KE}_t(k)$ and of the potential energy centroid $k_{APE} = \int dk\ k\widetilde{APE}(k)/\int dk\ \widetilde{APE}(k)$ in the case $rR/U = 0$. (b) Initial temporal evolution of the kinetic energy k-centroid of the upper layer and of the available potential energy k-centroid in the case $rR/U = 40$. Time is adimensionalized in both cases by $t_{adv} = L_y/U$.

The spontaneous emergence of ribbons also supports the argument of Subsection III C based on cascade phenomenology and on potential vorticity homogenization theory. Indeed, we see in Fig. 6(a) comparison between the temporal evolution of the kinetic and potential energy centroids both in the case $rR/U = 0$ (barotropic dynamics at lowest order) and $rR/U = 40$ ($1^1/_2$ layer quasi-geostrophic dynamics at lowest order). In the case with vanishing bottom friction, the kinetic energy centroid goes to the domain scale and remains there, as expected from inverse energy cascade arguments. In the case with high bottom friction, the centroid of potential energy initially goes to large scale, and so does the centroid of kinetic energy (slaved to the inverse cascade of potential energy). But once this centroid has reached the domain scale, the kinetic energy centroid goes back to smaller scale until a plateau is reached, while the potential energy centroid remains at large scale. This clearly indicates that streamlines are "pinched," or expelled at the boundary between regions of homogenized potential vorticity. It was shown by Dritschel and Scott[41] that such a jet sharpening mechanism through turbulent stirring is enhanced by the presence of coherent vortices in the vicinity of the jets. We actually observed the presence of such vortices for values of bottom friction rR/U large but of order one, but these vortices disappeared at large time for $rR/U > 10$.

The emergence of the ribbons as a potential homogenization process is conveniently described by a Hovmöller diagram of Fig. 7(a) showing the temporal evolution meridional slices of the potential vorticity profile $q_1(y,t)$ and by the temporal evolution of the global distribution of potential vorticity levels shown in Fig. 7(b). Clearly, the dynamics initially form multiple regions of homogenized potential vorticity with ribbons at their interfaces, and these regions eventually merge together until two regions of homogenized potential vorticity are formed.

2. Ribbon dynamics

We explained in Subsection III D 2 that statistical mechanics theory of the $1^1/_2$ layer model with small R/L_y predicts not only the ultimate formation of two regions of homogenized potential vorticity but also the organization of these regions into a configuration that minimizes the length of their interface. Clearly, the interface perimeter of the potential vorticity field in Fig. 5(d) is not minimal. Moreover, a movie would reveal that this interface is permanently meandering, and sometimes even breaks locally (see movie 3 in supplementary material[42]). Indeed, the jets at the interface between the regions of homogenized potential vorticity field are characterized by a strong vertical shear and are therefore expected to be baroclinically unstable. This instability is actually a mixed barotropic-baroclinic instability, since the jets have a horizontal structure. To check that the meanders were due to the existence of a vertical shear, we ran a numerical simulation of the

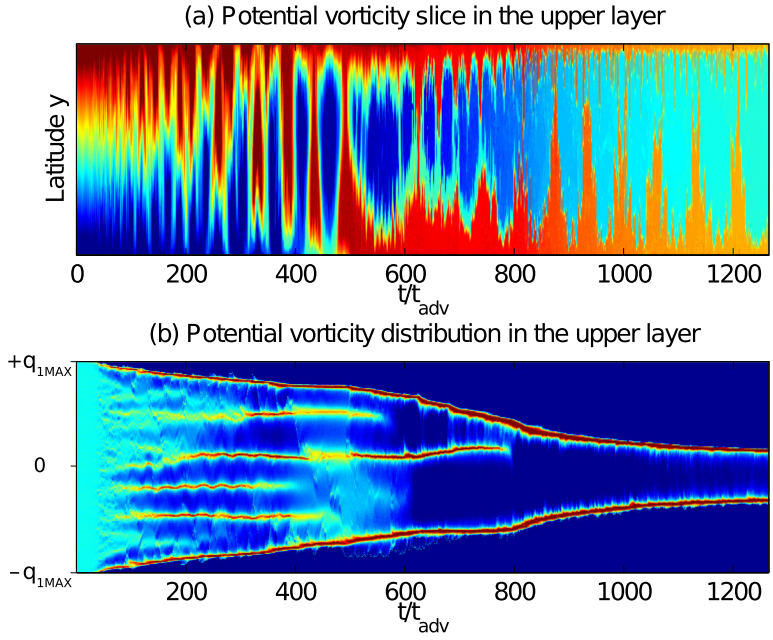

FIG. 7. (a) Hovmöller diagram of a potential vorticity line q(y,t) for a given longitude x in the large bottom friction run $rR/U = 40$. (b) Temporal evolution of the global distribution of potential vorticity levels in the same run. Time is adimensionalized by $t_{adv} = U/L_y$ in both cases.

$1^1/_2$ quasi-geostrophic dynamics taking the potential vorticity field of Fig. 5(d) as an initial condition. This amounts to imposing $\psi_2 = 0$ and therefore precludes any baroclinic instability. In those freely evolving simulations, the interface did stop meandering and the flow did reach a stationary state. We also observed that the interface was eventually smoothed out in the freely evolving $1^1/_2$ layer quasi-geostrophic simulations, while the interface remains sharp throughout the flow evolution when baroclinic instability is allowed, as seen on the Hovmöller diagram Fig. 7(a). We conclude that in the limit of large bottom friction, there is a competition between baroclinic instability that tends to increase the interface perimeter between regions of homogenized potential vorticity and the dynamics of the inviscid $1^1/_2$ layer quasi-geostrophic system that tends to minimize this interface.

Baroclinic instability of the ribbons is the mechanism that allows reduction little by little of the potential vorticity jumps across the ribbons, at a time scale given by $t_{diss} \sim rRL_y/(\delta^{1/2}U^2)$. This time scale is of the order of the slow variations of the potential vorticity interface at large time in the Hovmöller diagram Fig. 7(a). We see on Fig. 7 that once two regions of homogenized potential vorticity are formed, the value of the potential vorticity jump $\mathcal{Q}_{1jump}$ between the homogenized regions decreases exponentially, with an e-folding depth of the order of the decay time for the kinetic energy t_{diss}. The corresponding flow structure (i.e., meandering jets with a ribbon shape) remains the same, but the strength of the jet also decreases in time, since $U_{jet} \sim \delta^{1/2}R\mathcal{Q}_{1jump}$.

3. A competition between interface minimization and baroclinic instability

We show on Fig. 5(d) a case where two simply connected regions of homogenized potential vorticity are formed. When bottom friction is decreased from $rR/U = 40$ to $rR/U = 2.5$, we see on the histograms of potential vorticity levels in Fig. 3 that the global potential vorticity distribution still evolves to a state characterized by a double delta function. However, a snapshot of the potential vorticity field in Fig. 8(b) reveals that when rR/U is decreased, the two peaks in the potential vorticity distribution are associated with several unconnected blobs of regions with homogenized potential vorticity. The typical size of potential vorticity blobs decreases with lower bottom friction, while the total interface perimeter increases with lower bottom friction. Similarly, we observed that decreasing the ratio R/L_y for a given value of the bottom friction coefficient leads to an increase of

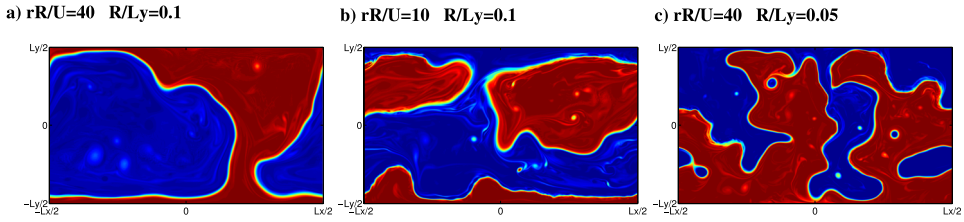

FIG. 8. Typical snapshots of the potential vorticity field (a) in the reference case (b) when bottom friction coefficient rR/U is decreased (c) when the Rossby radius R/L_y is decreased. The typical size of the potential vorticity blobs decreases from (a) to (c) and the interface perimeter increases from (a) to (c).

the interface perimeters between regions of homogenized potential vorticity, and to the detachment of isolated blobs of homogenized potential vorticity, see Fig. 8(c).

We interpret these observations by noting first that destabilization of the ribbons occurs at a time scale of the energy decay controlled by the baroclinic instability and given by $t_{diss} \sim (rRL_y/U^2)$ according to the large friction limit of Eqs. (20) and (21). By contrast, the tendency of the $1^1/_2$ quasi-geostrophic dynamics to form simply connected regions of homogenized potential vorticity with minimal interface occurs at a time scale t_{relax} independent from bottom friction parameter rR/U. To estimate t_{relax}, we assume first that the flow is composed of two "phases" characterized by different values of potential vorticity, but that there are several blobs associated with each phase (like bubbles in liquid water). The potential vorticity jump between these two phases can be estimated to be initially $\mathcal{Q}_1 \sim UL_y/\delta R^2$, which corresponds to stream function variations $\psi_1 \sim UL_y$. Let us introduce L_{flow}, the typical length scale of a blob of homogenized potential vorticity. Then, assuming $L_{flow} \gg \delta^{1/2}R$ and $L_{flow} \ll L_y$, and using the fact that the dynamics of the large scale flow is given at lowest order by the planetary quasi-geostrophic model Eq. (36), we obtain $\partial_t\psi_1/(\delta R^2) \sim J(\nabla^2\psi_1, \psi_1)$, which gives $\psi_1/(t_{relax}\delta R^2) \sim \psi_1^2/L_{flow}^4$. Using $\delta \sim 1$ and $\psi_1 \sim UL_y$, we obtain $t_{relax} \sim L_{flow}^4/(R^2L_yU)$. A quasi-stationary state is reached when the relaxation time scale is of the order of the baroclinic instability time scale given in Eq. (33), which yields

$$L_{flow} \sim L_y\left(\frac{rR}{U}\right)^{1/4}\left(\frac{R}{L_y}\right)^{1/2}. \tag{37}$$

The validity of scaling requires a scale separation that was not clear in our simulations (the potential vorticity blobs are not much smaller than the domain scale on Fig. 8). However, this naive scaling allows to interpret qualitatively our numerical results. The main point is that decreasing the bottom friction or the Rossby radius of deformation corresponds to a decrease of the typical size of L_{flow} isolated blobs of potential vorticity, which means an increase of the number of isolated blobs (since the goal area of a given phase is fixed), and therefore an increase of the total interface perimeter. We also note that the exponent $1/4$ means that variations of L_{flow} are very weak when bottom friction is changed over one or two decades such as in our simulations. Finally, we note that the length scale L_{flow} for the homogenized potential vorticity blobs can be interpreted as the scale of the available potential energy field, and that our scaling equation (37) is in very good agreement with the variations of the potential energy centroid when bottom friction is varied in numerical simulation by Arbic and Flierl[9] (Figure 9(a) of their paper).

4. Multiple jets

We show in Fig. 7(b) that there is a transient regime with multiple peaks in the global potential vorticity distribution. These transient states correspond initially to multiple regions of homogenized potential vorticity. We found that in the ribbon regime, the number of long lasting multiple regions of homogenized potential vorticity increased: (i) when the domain aspect ratio L_x/L_y was decreased, (ii) when bottom friction rR/U was increased, and (iii) when the parameter R/L_y was decreased. In addition, when the parameter R/L_y was sufficiently small, the regions of homogenized potential vorticity are initially organized into zonal bands with eastward jets at their

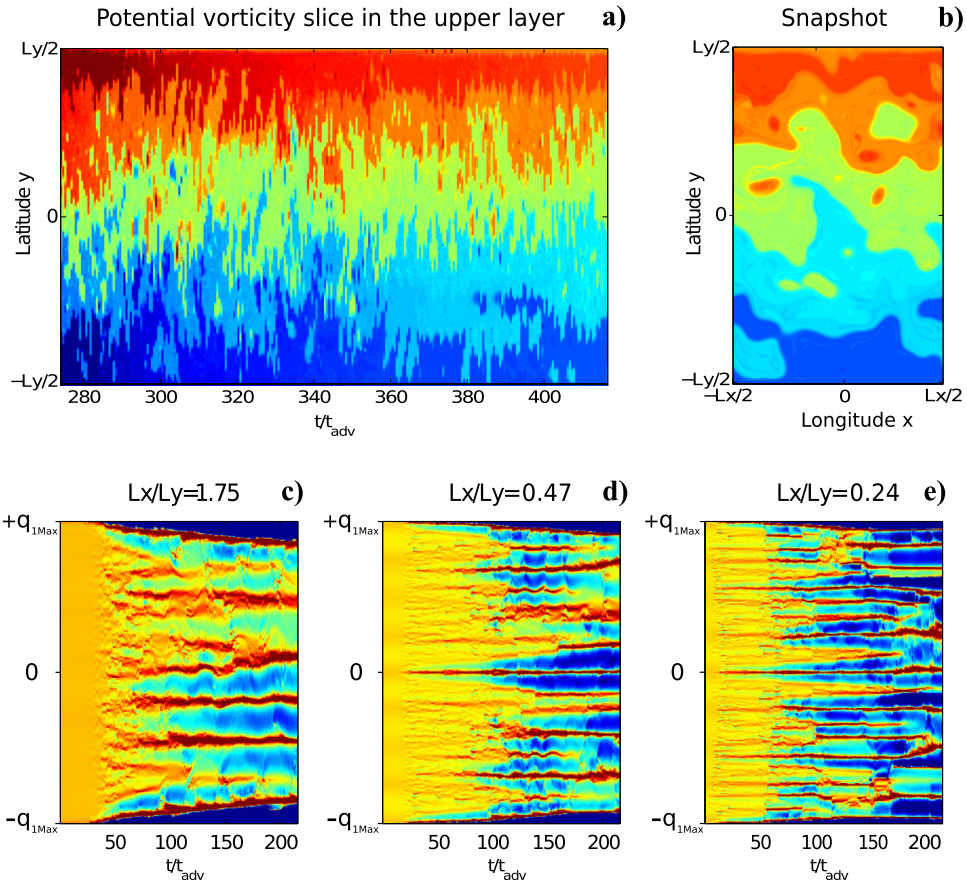

FIG. 9. Multiple jets as a transient regime towards complete homogenization. (a) Hovmöller diagrams of a meridional slice of the potential vorticity field in the upper layer, time is renormalized by $t_{adv} = L_y/U$. (b) Typical snapshot of the potential vorticity field in the upper layer. (c), (d), and (e) Evolution of the global distribution of potential vorticity levels in the upper layer for different values of the domain aspect ratio, $L_x/L_y = 1.75$, 0.47, and 0.24, respectively. All those runs are performed in the large bottom friction limit $rR/u = 40$.

interface, which is reminiscent of potential vorticity staircases.[43] We show in Figs. 9(a) and 9(b) an example of such long lasting multiple zonal bands of potential vorticity. In addition, Figs. 9(c)–9(e) show how the number of regions of homogenized potential vorticity increases with smaller domain aspect ratio L_x/L_y. It is not clear whether the dynamics would eventually form only two regions of homogenized potential vorticity, or if more than two regions of homogenized potential vorticity could last for ever. One may interpret qualitatively the emergence of these potential vorticity staircases by noticing that once a jet is formed between two regions of homogenized potential vorticity, it acts as a strong mixing barrier between the two adjacent regions, which may prevent further mixing with other regions of homogenized potential vorticity. We note that in our case there is no beta effect. The zonal organization of the potential vorticity field only reflects the structure of the prescribed eastward jet, which induces an effective beta effect in the upper layer.

The existence of long lived multiple eastward jets provides a route towards potential vorticity homogenization that sustains a total eastward transport of the order of the transport of the prescribed eastward jet. This contrasts with the low or intermediate bottom friction case where the rapid decrease of the total potential energy (over a time $t_{adv} = L_y/U$) is accompanied with a rapid decrease of the total zonal transport. In that respect, we find that increasing bottom friction leads to an increasing zonal transport in the regime where multiple jets are allowed. Increasing transport associated with increasing bottom friction was reported in the context of idealized simulations of

the Antarctic circumpolar circulation,[44] but this effect was due to the presence of bottom topography which is absent in our simulations.

We finally note that multiple jets separating regions of homogenized several regions of homogenized potential vorticity are not *a priori* excluded from statistical mechanics predictions. Indeed, it is conjectured in Bouchet and Sommeria[12] that the case with two regions of homogenized potential should occur for most initial potential vorticity distribution and initial energies, but that other cases may be possible. For instance, high energy states associated with a global distribution of potential vorticity presenting n peaks will lead to a state with n regions of homogenized potential vorticity separated by sharp jets at their interface.

V. CONCLUSION

We have presented numerical simulations for the non-linear equilibration of a two-layer quasi-geostrophic flow in a channel in the presence of a prescribed baroclinically unstable flow U in the upper layer with particular attention to the role of bottom friction. For any nonzero value of the bottom friction coefficient, r, the dynamics attempts to homogenize the potential vorticity field, including any large scale gradient due to the prescribed eastward flow in the upper layer, as might be expected from classical theories of geostrophic turbulence.[45] However, the route toward complete homogenization depends strongly on the bottom friction coefficient.

When the bottom friction is weak ($r \ll U/R$), the perturbation self-organizes at the domain scale into a quasi-barotropic large scale structure (see movie 1 in supplementary material[42]), which is then weakly dissipated on a time scale inversely proportional to the bottom friction coefficient, $t_{diss} \sim 1/r$. We interpret this large-scale quasi-stationary flow as a statistical equilibrium state of the MRS theory.

When the bottom friction has a medium value, meaning that its time scale is of the order of the inviscid baroclinic instability time scale ($r \sim U/R$), bottom friction precludes an inverse kinetic energy cascade close to the injection length scale (which is of the order of the Rossby radius deformation R) and the dynamics is well described by a gas of isolated vortices of size R mixing the background potential vorticity field at the advection time scale $t_{diss} \sim L_y/U$ (see movie 2 in supplementary material[42]).

When the bottom friction coefficient is high ($r \gg U/R$), the ratio between the lower layer kinetic energy and the upper layer kinetic energy scales as $(rR/U)^2$ and the dynamics is well described at lowest order by a $1^1/_2$ layer quasi-geostrophic model. We observed the spontaneous emergence of meandering ribbons corresponding to strong jets of width given by the Rossby radius of deformation of the upper layer and separating regions of homogenized potential vorticity (see movie 3 in supplementary material[42]). We used statistical mechanics arguments as well as cascade phenomenology to interpret these results. We described a competition between the inviscid $1^1/_2$ quasi-geostrophic dynamics that tends to form only two regions of homogenized potential vorticity with a minimal interface between them and baroclinic instability of the ribbons that tends to increase the interface perimeter. This last route towards potential vorticity homogenization is rather spectacular: the potential vorticity jump between the two regions of homogenized potential vorticity decreases slowly with time, due to the intermittent breaking of the ribbons at their interface. This process occurs at a time scale given by baroclinic instability that scales linearly with the bottom friction coefficient $t_{diss} \sim rRL_y/U^2$. Remarkably, the interface between the homogenized regions of potential vorticity remains sharp (i.e., much smaller than the Rossby radius of deformation) throughout this evolution towards a single, fully homogenized potential vorticity field.

Using cascade phenomenology, and generalizing the arguments by Held and Larichev,[39] Arbic and Flierl[9] proposed scalings for the horizontal scale and the vertical structure of the dynamics in the large friction regime. Here we obtained rather different scalings, but with similar qualitative meaning, by assuming that the flow structures resulted from the competition between baroclinic instability and a tendency to reach a Miller-Robert-Sommeria equilibrium state in both the weak and the large bottom friction limits. We believe that the cascade arguments are more suited to

intermediate bottom friction, for which there is a scale separation between the large scale flow and the perturbed flow.

A key novelty of our work is to relate the condensation of kinetic energy into ribbons with existing statistical predictions for the $1\frac{1}{2}$ layer quasi-geostrophic model and to provide a complementary argument based on cascade phenomenology. The fact that arguments derived from cascade phenomenology lead to the same prediction as equilibrium statistical mechanics is very striking in this example. More generally, since one approach describes kinetics of energy transfers and the other describes the final invariant measure in the same flow model, they should both give a consistent picture.

In addition, we show for the first time numerical evidence that when the Rossby radius of deformation is much smaller than the domain scale, the dynamics attracts the system towards a quasi-stationary state characterized by a tanh-like relation between potential vorticity and stream function, even if the initial potential vorticity distribution is not already made of several regions with homogenized potential vorticity. We note that in our case the presence of two layers was essential to observe large regions of homogenized potential vorticity, even if the dynamics is described at lowest order by a $1\frac{1}{2}$ layer quasi-geostrophic flow. Indeed, the presence of the bottom layer allows for baroclinic instability of the ribbons, which favors stirring of the upper layer potential vorticity field in the whole flow domain. By contrast, once a ribbon emerges in a freely evolving $1\frac{1}{2}$ quasi-geostrophic flow, it acts as a mixing barrier that prevents further exchanges between adjacent regions of homogenized potential vorticity.

Our work was set in a channel geometry in which case the global distribution of a suitably defined potential vorticity field is conserved in the absence of small scale dissipation. This allows us to use statistical mechanics arguments and reinterpret the results obtained in previous work in doubly periodic geometry. Thus, in the large bottom friction limit, the dissipation time $t_{diss} \sim rRL_y/U^2$ can be interpreted as an intrinsic time scale for the variability of the available potential energy in a statistically steady state. It is also interesting to compare our results with those of Esler,[46] Willcocks and Esler,[47] who considered the free evolution of a surface intensified zonal jet localized at the center of a channel. In their case, the instability is localized around the jet, and potential vorticity stirring occurs only within this central region. Statistical mechanics predictions fail in this case to predict the large scale flow structure since the dynamics does only explore a restricted part of the phase space. By contrast, in our simulations, the initial instability and its subsequent turbulent evolution takes place in the whole domain, which induces potential vorticity stirring everywhere, excepted when multiple jets occur.

To conclude, this study shows that large bottom friction induces the condensation of the kinetic energy into quasi-stationary ribbons and the concomitant condensation of potential energy at large scale. Perhaps paradoxically increasing the bottom friction considerably slows down the loss of energy from the potential energy reservoir associated with the large scale flow.

The regime for ribbon turbulence requires bottom friction coefficients which are too high for a direct application to oceanic flows. However, other physical mechanisms than bottom drag may be able to remove energy from the lower layer, which would mimic the effect of high bottom friction. For instance LaCasce and Brink[48] showed in the framework of freely decaying two-layer quasi-geostrophic turbulence over a slope that topographic Rossby waves generated in some locations remove the energy to other locations, where it eventually is dissipated by bottom drag. This effect may me interpreted as an enhanced bottom friction in the region where the topographic wave is generated.

Further work will be needed to extend these results to continuously stratified fluids because in that case other effects can significantly change the properties of the vertical structure of the eddies, see Smith and Vallis,[49] Roullet *et al.*[50] for the forced dissipated case and Smith and Vallis[51] for the freely evolving case. In particular, Smith and Vallis,[51] Fu and Flierl[52] did show that in the presence of surface intensified stratification, and without bottom friction, there is a fast time scale associated with energy transfers toward the first baroclinic mode. This energy eventually condenses into the barotropic mode, but with a much larger time scale. The beta effect may also have several consequences: it is known to favor barotropization[18] and to favor the arrangement of regions of homogenized potential vorticity into zonal bands.

We focused in this paper on the non-linear equilibration of a perturbation around a prescribed eastward jet. We explained that in a channel geometry, the dynamics is equivalent to a free decay experiment in which the initial condition is the prescribed jet. It would be useful to generalize these results to a more realistic setting with forcing by considering for instance a surface wind stress. The large scale baroclinic velocity U appearing in the non-dimensional parameter rR/U will have to be related to the forcing case by case.

ACKNOWLEDGMENTS

We thank David Straub for useful discussions and two anonymous reviewers for numerous suggestions that helped to improve the presentation. A.V. was funded by ANR LORIS (ANR-10 -CEXC-010-01) during part of this work.

APPENDIX: BAROTROPIZATION IN THE WEAK BOTTOM FRICTION LIMIT

The aim of this appendix is to give a phenomenological argument for barotropization when $R \ll L_y$, with $L_x \sim L_y$ and $\delta \sim 1$. The argument is based on the fact that turbulence leads to a rearrangement of the initial potential field in each layer, with a constant total energy E_{tot}.

The global distribution of potential vorticity levels in both layers is conserved when there is neither small scale dissipation nor bottom friction.

Let us call $\mathcal{Q}_1$ the typical variations of the potential vorticity field in the upper layer after turbulent rearrangement of the initial field $q_1^0 = Uy/(\delta R^2)$. We see Eq. (24) that typical variations of the barotropic streamfunction are given by $\psi_t \sim \delta L_y^2 \mathcal{Q}_1$, where we anticipate that the typical length scale of flow structures in this regime is given by the domain size L_y. We also see from Eq. (23) that typical variations of the baroclinic streamfunction are $(\psi_c - Uy) \sim R^2 \mathcal{Q}_1$ over a length R when $R \ll L_y$. With these estimates, and anticipating that $\psi_t \gg Uy$, we find the following scalings for the different components of the energy of the perturbed flow introduced Eq. (27),

$$KE_{tot,t} \sim \mathcal{Q}_1^2 L_y^4, \quad KE_{tot,c} \sim \mathcal{Q}_1^2 R^3 L_y, \quad APE_{tot,c} \sim \mathcal{Q}_1^2 R^2 L_y^2. \tag{38}$$

Clearly, the total energy $E_{tot} = KE_{tot,t} + KE_{tot,c} + APE_{tot,c}$ is dominated by its barotropic component $KE_{tot,t}$ when $R \ll L_y$. Since the barotropic dynamics leads to an inverse kinetic energy cascade, our hypothesis that L_y is a typical scale of the flow is self-consistent. Using the estimate of the initial energy $E_{tot}^0 \sim APE_{tot}^0 \sim U^2 L_y^4/R^2$, and using the fact that this energy is fully transferred into the barotropic mode after turbulent rearrangement, we get $KE_{tot,t} \sim U^2 L_y^4/R^2$. Using Eq. (38), this estimate yields $\mathcal{Q}_1 \sim U/R$. Consequently, the order of magnitude for the barotropic velocity is $U_t \sim UL_y/R$, which is consistent with the hypothesis that $\psi_t \gg Uy$. We conclude that the total flow is dominated by the barotropic component of the flow $R \ll L_y$ after turbulent rearrangement of the potential vorticity field, and that this barotropic flow is characterized by velocities much larger than the velocity of the initial eastward jet.

[1] I. M. Held, "The gap between simulation and understanding in climate modeling," Bull. Am. Meteorol. Soc. **86**, 1609–1614 (2005).
[2] A. C. de Verdiere, "Keeping the freedom to build idealized climate models," Eos, Trans. Amer. Geophys. Union **90**, 224 (2009).
[3] G. K. Vallis, *Atmospheric and Oceanic Fluid Dynamics* (Cambridge University Press, 2006).
[4] J. G. Charney, "Geostrophic turbulence," J. Atmos. Sci. **28**, 1087–1095 (1971).
[5] P. B. Rhines, "Geostrophic turbulence," Annu. Rev. Fluid Mech. **11**, 401–441 (1979).
[6] R. Salmon, *Lectures On Geophysical Fluid Dynamics* (Oxford University Press, 1998).
[7] A. F. Thompson and W. R. Young, "Scaling baroclinic eddy fluxes: Vortices and energy balance," J. Phys. Oceanogr. **36**, 720 (2006).
[8] B. K. Arbic and G. R. Flierl, "Coherent vortices and kinetic energy ribbons in asymptotic, quasi two-dimensional f-plane turbulence," Phys. Fluids **15**, 2177–2189 (2003).
[9] B. K. Arbic and G. R. Flierl, "Baroclinically unstable geostrophic turbulence in the limits of strong and weak bottom Ekman friction: Application to midocean eddies," J. Phys. Oceanogr. **34**, 2257–2273 (2004).
[10] J. Miller, "Statistical mechanics of Euler equations in two dimensions," Phys. Rev. Lett. **65**, 2137–2140 (1990).
[11] R. Robert and J. Sommeria, "Statistical equililbrium states for two-dimensional flows," J. Fluid Mech. **229**, 291–310 (1991).
[12] F. Bouchet and J. Sommeria, "Emergence of intense jets and Jupiter's great red spot as maximum-entropy structures," J. Fluid Mech. **464**, 165–207 (2002).

[13] J. Pedlosky, *Geophysical Fluid Dynamics* (Springer-Verlag, New York and Berlin, 1982), Vol. 1, p. 636.
[14] J. C. McWilliams, W. R. Holland, and J. Chow, "A description of numerical Antarctic Circumpolar Currents," Dyn. Atmos. Oceans **2**, 213–291 (1978).
[15] W. R. Holland, "The role of mesoscale eddies in the general circulation of the ocean-numerical experiments using a wind-driven quasi-geostrophic model," J. Phys. Oceanogr. **8**, 363–392 (1978).
[16] T. G. Shepherd, "Nonlinear saturation of baroclinic instability. Part I: The two-layer model," J. Atmos. Sci. **45**, 2014–2025 (1988).
[17] The potential vorticity of a fluid particle in the lower layer is $q_2 = \nabla^2\psi_2 + (\psi_1 - \psi_2 - U\,y)/((1-\delta)R^2)$; the term $(\psi_2 - \psi_1)/\delta R^2$ may be expected to remain bounded since streamfunctions are smooth fields, and the total energy is bounded. Consequently, if q_2 becomes very large, then $q_2 \approx \nabla^2\psi_2$, and bottom friction will tend to decrease the value of q_2.
[18] A. Venaille, G. Vallis, and S. Griffies, "The catalytic role of the beta effect in barotropization processes," J. Fluid Mech. **709**, 490–515 (2012).
[19] A. Venaille, "Mélange et circulation océanique: Une approche par la physique statistique," Ph.D. thesis (Université Joseph Fourier-Grenoble, 2008).
[20] C. Herbert, "Nonlinear energy transfers and phase diagrams for geostrophically balanced rotating-stratified flows," Phys. Rev. E **89**, 033008 (2014).
[21] R. Fjortoft, "On the changes in the spectral distribution of kinetic energy for two-dimensional non-divergent flow," Tellus **5**, 225–230 (1953).
[22] R. H. Kraichnan, "Inertial ranges in two-dimensional turbulence," Phys. Fluids **10**, 1417 (1967).
[23] S. Nazarenko and B. Quinn, "Triple cascade behavior in quasi-geostrophic and drift turbulence and generation of zonal jets," Phys. Rev. Lett. **103**, 118501 (2009).
[24] V. D. Larichev and J. C. McWilliams, "Weakly decaying turbulence in an equivalent-barotropic fluid," Phys. Fluids **3**, 938–950 (1991).
[25] R. T. Pierrehumbert, I. M. Held, and K. L. Swanson, "Spectra of local and nonlocal two-dimensional turbulence," Chaos Solitons Fractals **4**, 1111–1116 (1994).
[26] K. S. Smith, G. Boccaletti, C. C. Henning, I. Marinov, C. Y. Tam, I. M. Held, and G. K. Vallis, "Turbulent diffusion in the geostrophic inverse cascade," J. Fluid Mech. **469**, 13–48 (2002).
[27] J. Miller, P. B. Weichman, and M. Cross, "Statistical mechanics, Eulers equation, and Jupiters red spot," Phys. Rev. A **45**, 2328 (1992).
[28] A. Majda and X. Wang, *Nonlinear Dynamics and Statistical Theories for Basic Geophysical Flows* (Cambridge University Press, 2006).
[29] J. Marston, "Planetary atmospheres as nonequilibrium condensed matter," Annu. Rev. Condens. Matter Phys. **3**, 285–310 (2012).
[30] F. Bouchet and A. Venaille, "Statistical mechanics of two-dimensional and geophysical flows," Phys. Rep. **515**, 227–295 (2012).
[31] V. Lucarini, R. Blender, C. Herbert, S. Pascale, and J. Wouters, "Mathematical and physical ideas for climate science," preprint arXiv:1311.1190 (2013).
[32] P. Chavanis and J. Sommeria, "Classification of self-organized vortices in two-dimensional turbulence: The case of a bounded domain," J. Fluid Mech. **314**, 267–298 (1996).
[33] A. Venaille and F. Bouchet, "Solvable phase diagrams and ensemble inequivalence for two-dimensional and geophysical turbulent flows," J. Stat. Phys. **143**, 346–380 (2011).
[34] M. Corvellec, "Phase transitions in two-dimensional and geophysical turbulence," Ph.D. thesis (Ecole Normale Superieure de Lyon, 2012).
[35] P. B. Weichman, "Equilibrium theory of coherent vortex and zonal jet formation in a system of nonlinear Rossby waves," Phys. Rev. E **73**, 036313 (2006).
[36] A. Venaille and F. Bouchet, "Oceanic rings and jets as statistical equilibrium states," J. Phys. Oceanogr. **41**, 1860–1873 (2011).
[37] L.-P. Nadeau and D. N. Straub, "Basin and channel contributions to a model Antarctic Circumpolar Current," J. Phys. Oceanogr. **39**, 986–1002 (2009).
[38] A. Arakawa, "Computational design for long-term numerical integration of the equations of fluid motion: Two-dimensional incompressible flow. Part I," J. Comput. Phys. **1**, 119–143 (1966).
[39] I. M. Held and V. D. Larichev, "A scaling theory for horizontally homogeneous, baroclinically unstable flow on a beta plane," J. Atmos. Sci. **53**, 946–952 (1996).
[40] D. Schecter, D. Dubin, K. Fine, and C. Driscoll, "Vortex crystals from 2d Euler flow: Experiment and simulation," Phys. Fluids **11**, 905 (1999).
[41] D. Dritschel and R. Scott, "Jet sharpening by turbulent mixing," Philos. Trans. R. Soc., A **369**, 754–770 (2011).
[42] See supplementary material available at http://dx.doi.org/10.1063/1.4904878 for Movie 1 shows the temporal evolution of the kinetic energy field and of the potential vorticity field in the upper layer and in the lower layer, in a case without bottom friction ($rR/U = 0$). There is a concomitant inverse cascade of kinetic energy on the horizontal with barotropization on the vertical. Movie 2 shows the same fields in the case of intermediate bottom friction ($rR/U \sim 1$), which leads to surface intensified point vortices with a typical horizontal length scale given by the Rossby radius of deformation. Movie 3 shows the same fields in the case of large bottom friction ($rR/U \gg 1$), which leads to the emergence of ribbons (meandering surface intensified sharp jets).
[43] D. Dritschel and M. McIntyre, "Multiple jets as PV staircases: The Phillips effect and the resilience of eddy-transport barriers," J. Atmos. Sci. **65**, 855–874 (2008).
[44] L.-P. Nadeau and D. N. Straub, "Influence of wind stress, wind stress curl, and bottom friction on the transport of a model Antarctic Circumpolar Ccurrent.," J. Phys. Oceanogr. **42**, 207–222 (2012).

[45] P. B. Rhines and W. R. Young, "Homogenization of potential vorticity in planetary gyres," J. Fluid Mech. **122**, 347–367 (1982).
[46] J. Esler, "The turbulent equilibration of an unstable baroclinic jet," J. Fluid Mech. **599**, 241–268 (2008).
[47] B. Willcocks and J. Esler, "Nonlinear baroclinic equilibration in the presence of Ekman friction," J. Phys. Oceanogr. **42**, 225–242 (2012).
[48] J. LaCasce and K. Brink, "Geostrophic turbulence over a slope," J. Phys. Oceanogr. **30**, 1305–1324 (2000).
[49] K. S. Smith and G. K. Vallis, "The scales and equilibration of midocean eddies: Forced-dissipative flow," J. Phys. Oceanogr. **32**, 1699–1720 (2002).
[50] G. Roullet, J. C. McWilliams, X. Capet, and M. J. Molemaker, "Properties of steady geostrophic turbulence with isopycnal outcropping," J. Phys. Oceanogr. **42**, 18–38 (2012).
[51] K. S. Smith and G. K. Vallis, "The scales and equilibration of midocean eddies: Freely evolving flow," J. Phys. Oceanogr. **31**, 554–571 (2001).
[52] L.-L. Fu and G. R. Flierl, "Nonlinear energy and enstrophy transfers in a realistically stratified ocean," Dyn. Atmos. Oceans **4**, 219–246 (1980).